



Studying Heavy-Ion Collisions with Electromagnetic Probes

Xiang-Yu Wu

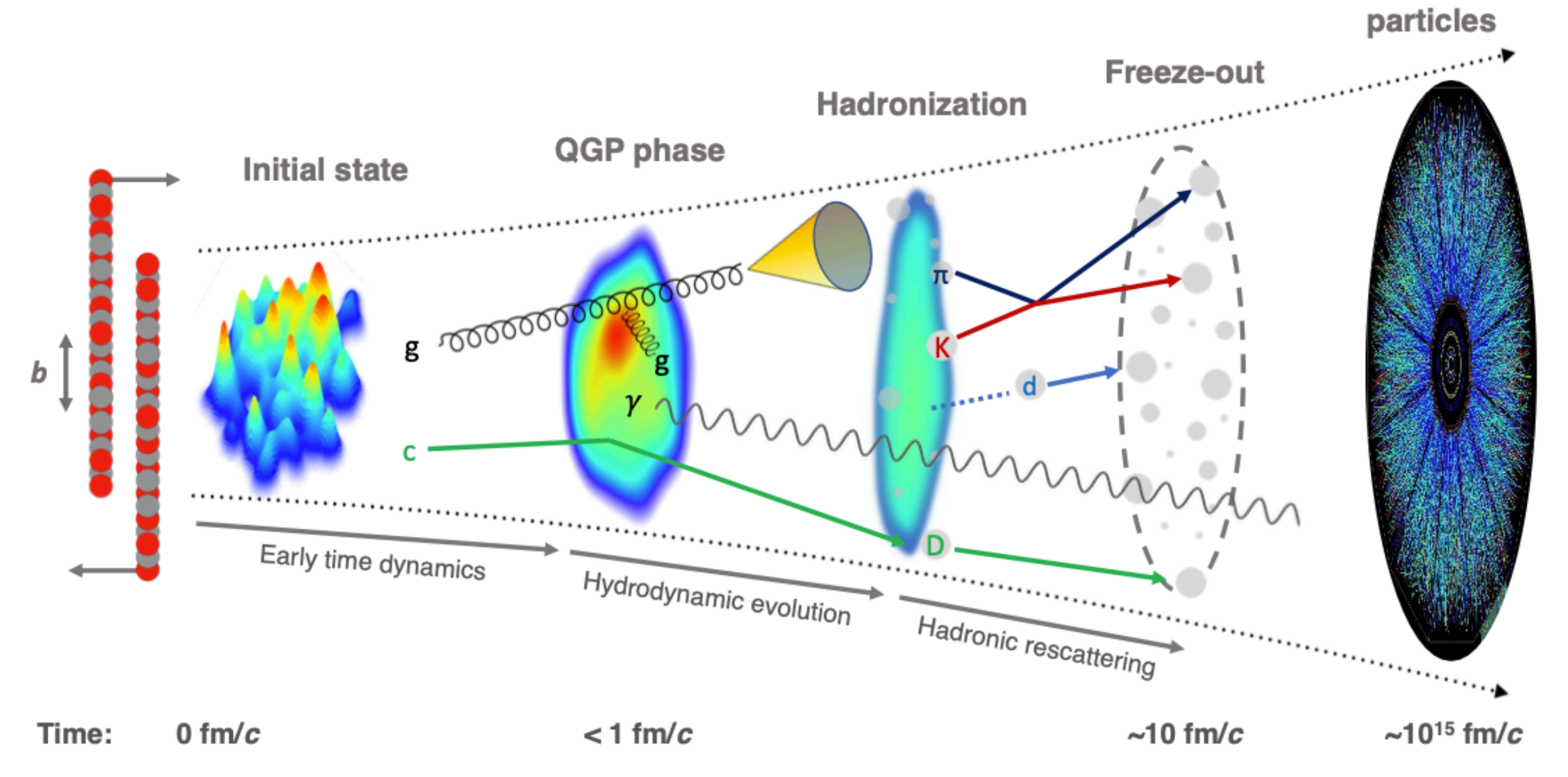
McGill University

The 234th HENPIC Seminar Oct. 16. 2025

Outline

- Introduction
- Dileptons in the Pre-equilibrium Stage
- Dilepton polarization
- Dilepton and photons at RHIC-BES
- Summary

Heavy ion collision



• Goals:

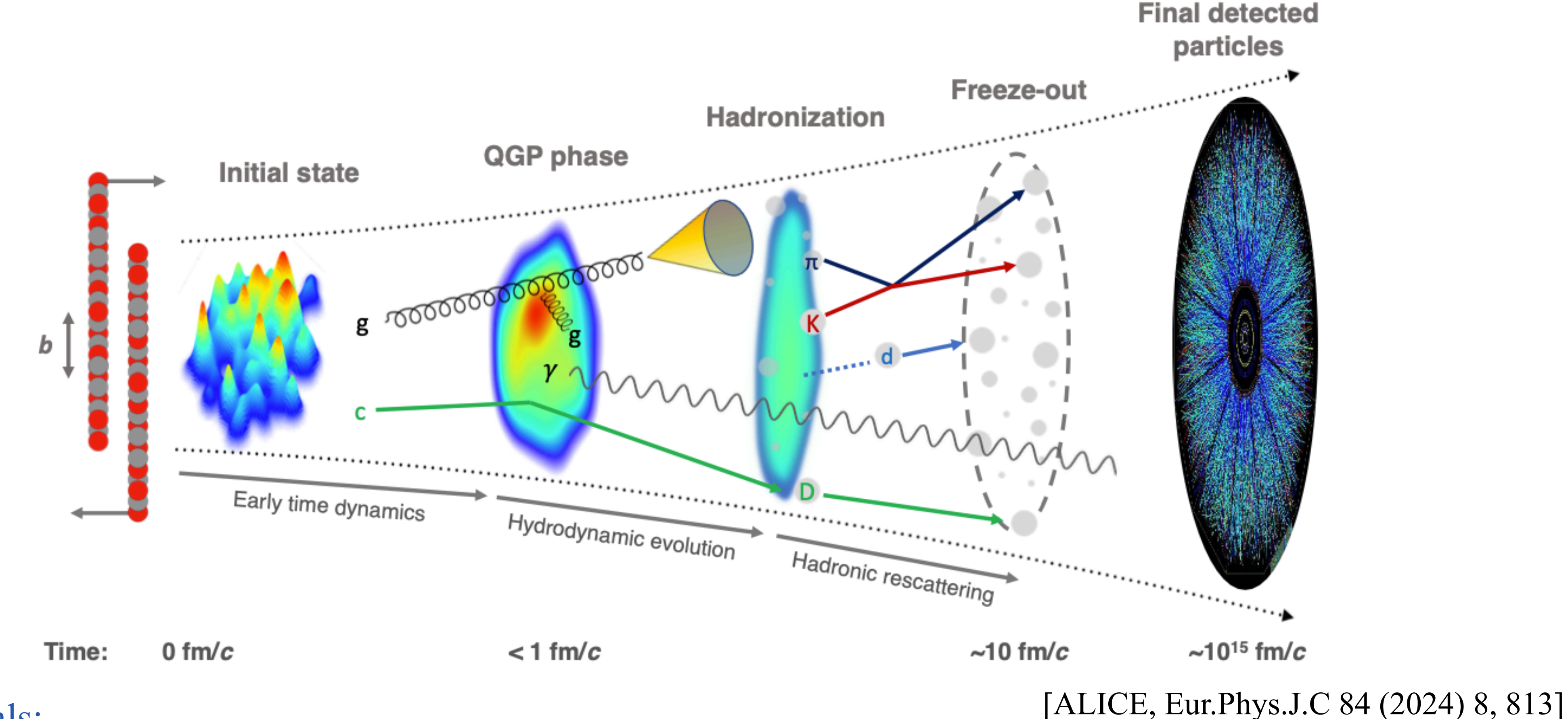
• Understand the initial conditions.

• Extract QGP transport coefficients.

[ALICE, Eur.Phys.J.C 84 (2024) 8, 813]

Final detected

Heavy ion collision

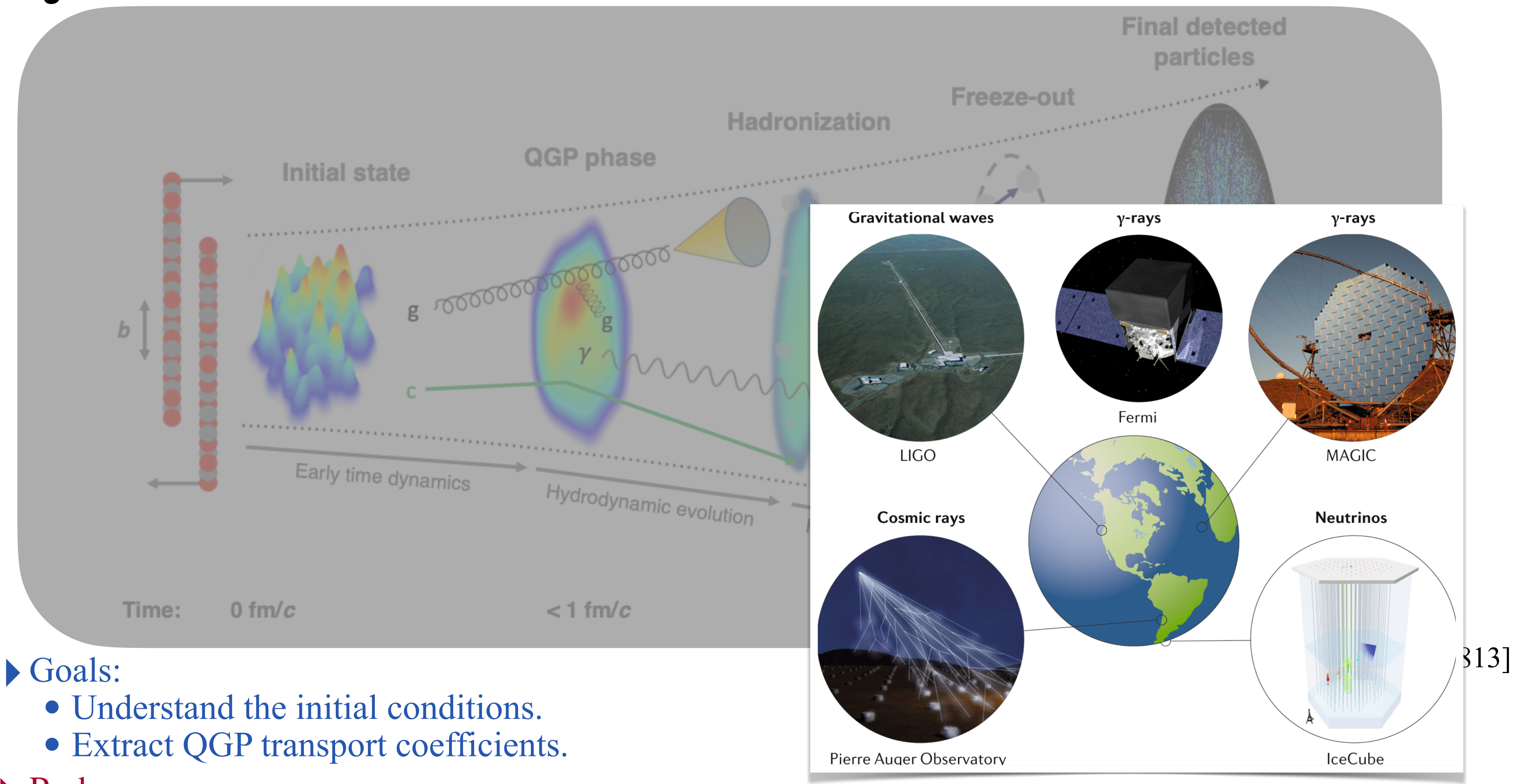


Goals:

- Understand the initial conditions.
- Extract QGP transport coefficients.
- Probes:
 - Soft hadrons, hard probes (high-pT hadrons and Jets), EM probes $(\gamma/l\bar{l})$.

Multi-messenger study

Heavy ion collision



Probes:

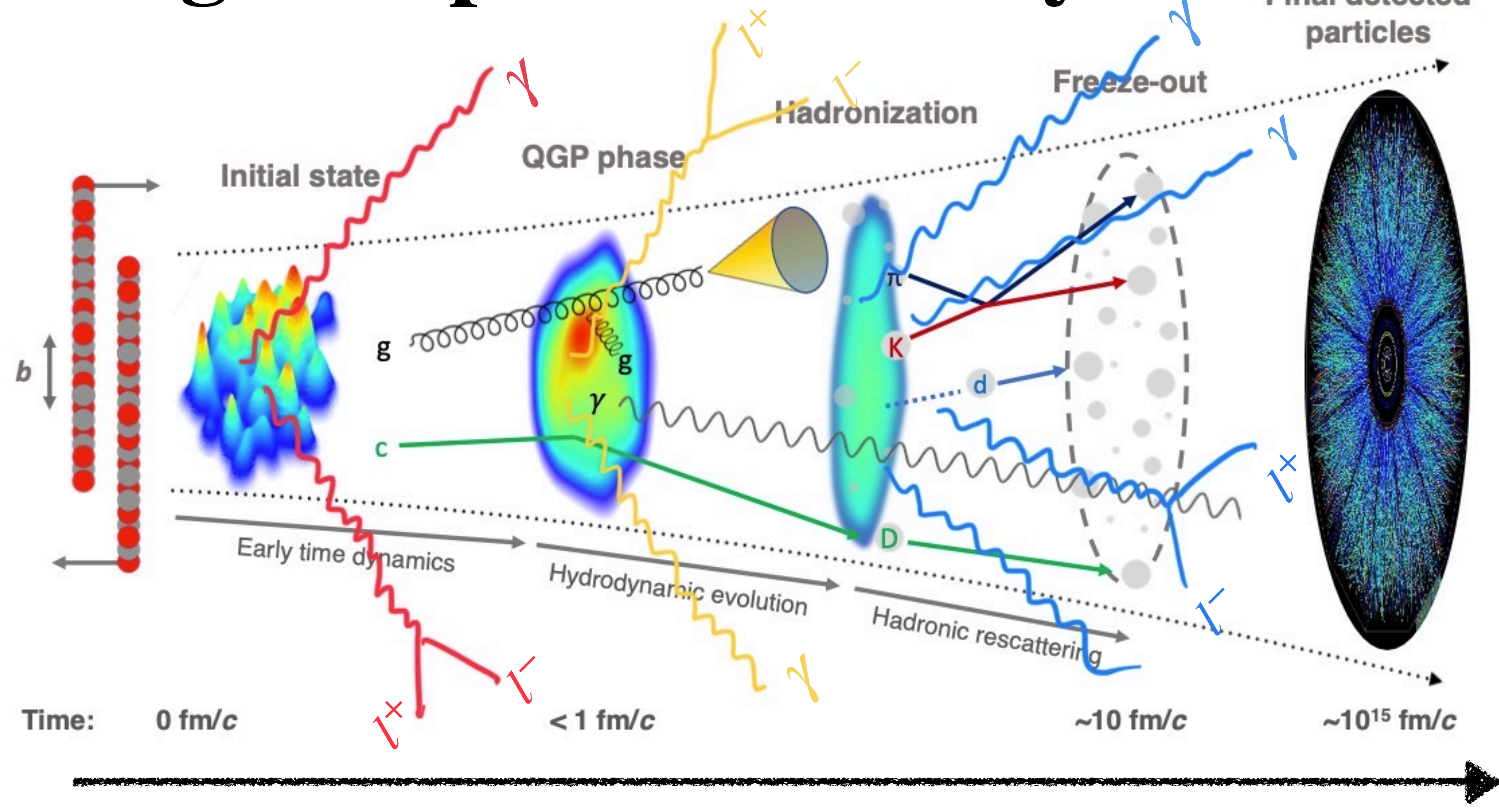
• Soft hadrons, hard probes (high-pT hadrons and Jets), EM probes ($\gamma/l\bar{l}$).



[Nature Rev.Phys. 1 (2019) 585-599]

Multi-messenger study

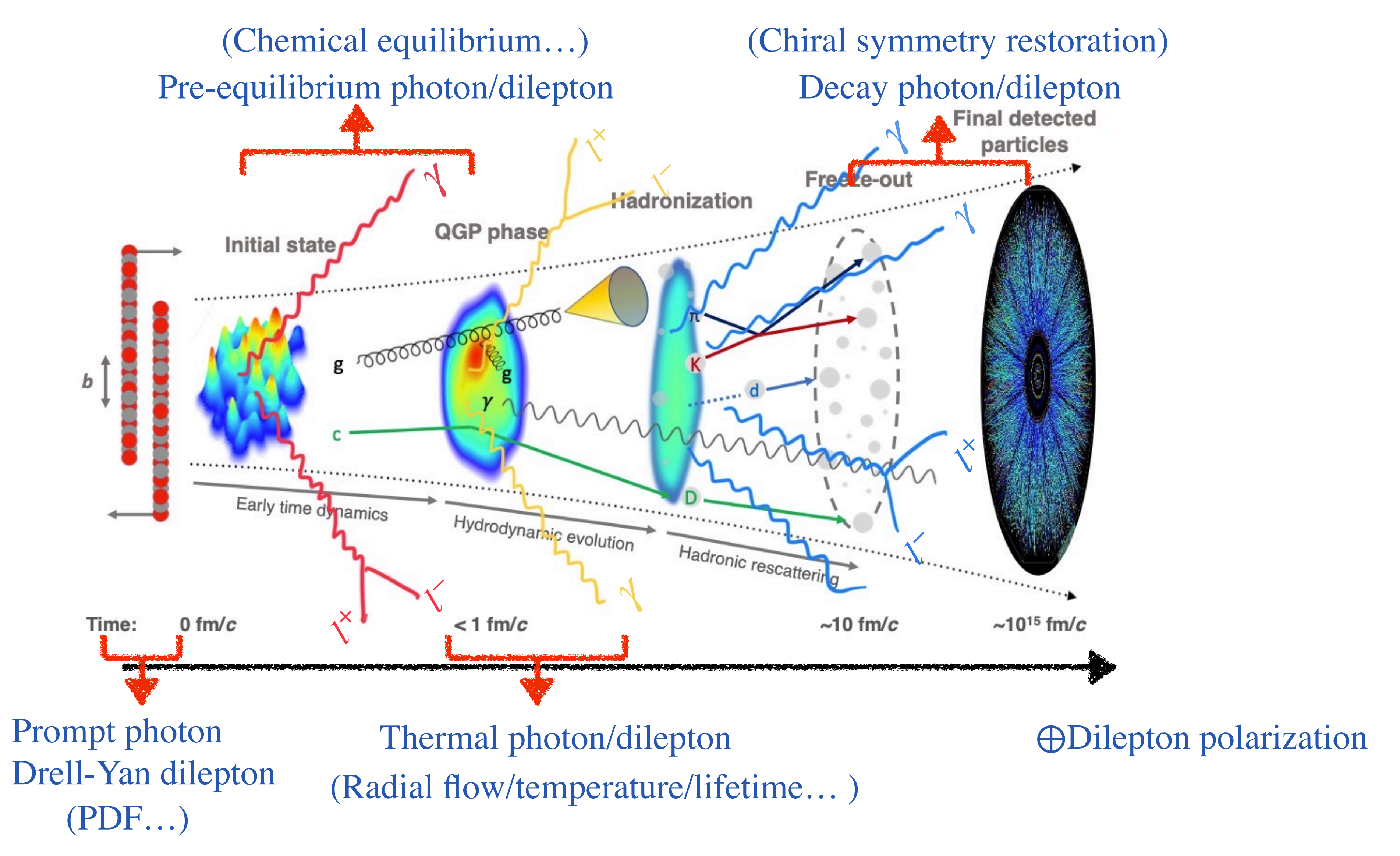
Electromagnetic probes in heavy ion collision



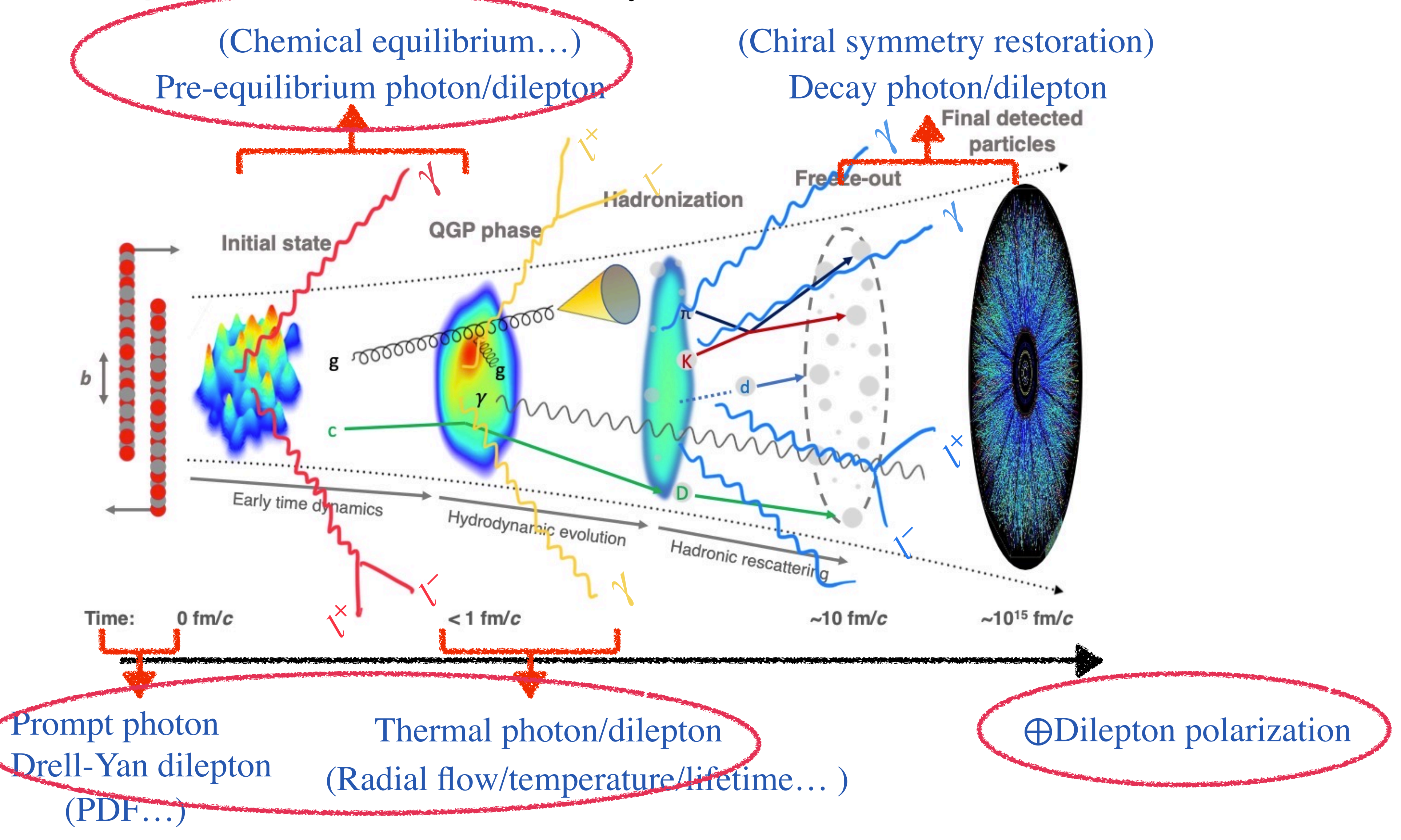
[ALICE, Eur.Phys.J.C 84 (2024) 8, 813]

- Electromagnetic probes $(\gamma/l\bar{l})$
 - Emitted throughout the entire evolution of heavy-ion collisions.
 - Penetrate the strongly interacting QGP medium without further interaction.
 - Carry details about the local production point.

Electromagnetic sources (γ/ll)



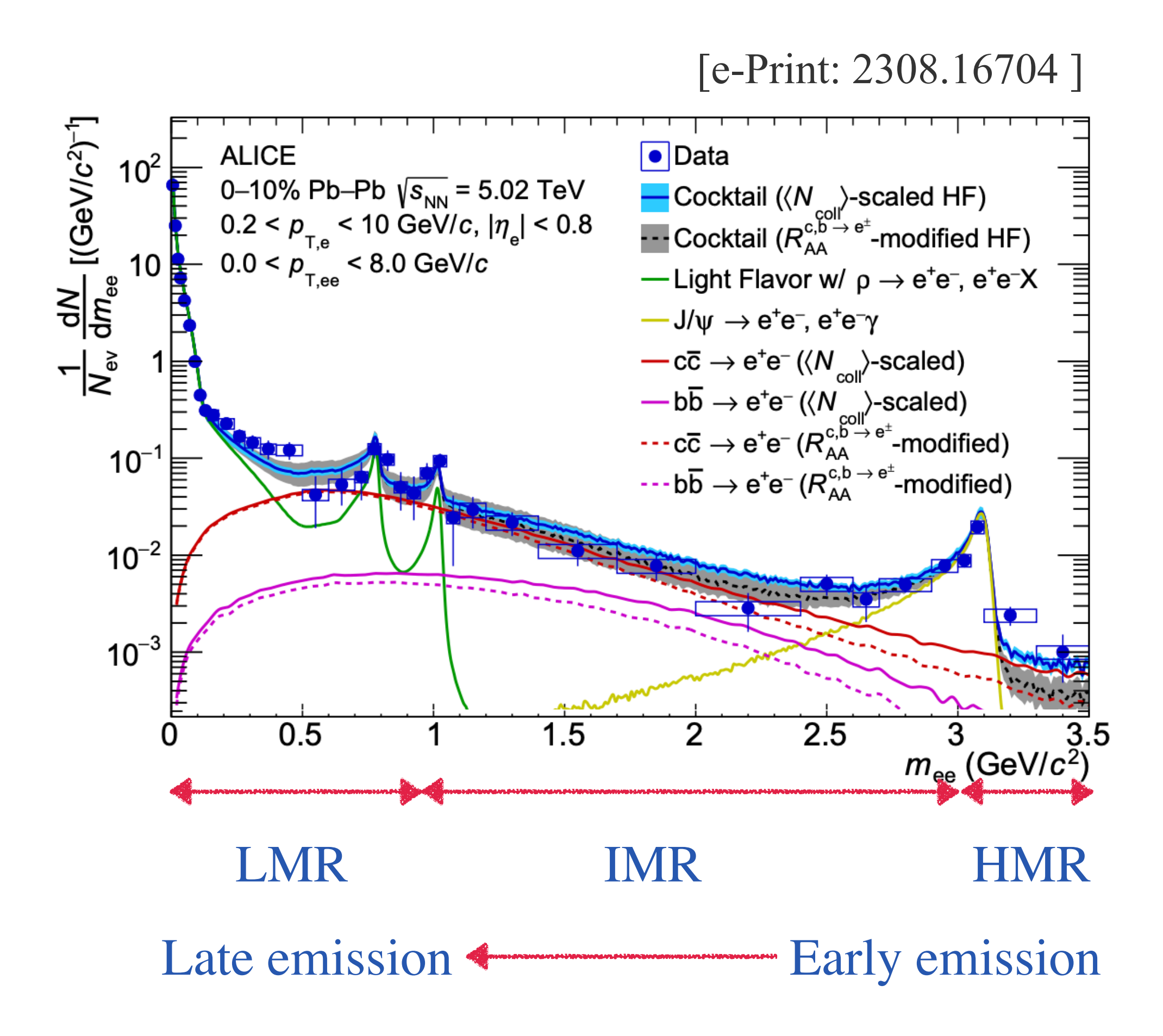
Electromagnetic sources (y/ll)



Outline

- Introduction
- Dileptons in the Pre-equilibrium Stage
- Dilepton polarization
- Dilepton and photons at RHIC-BES
- Summary

Why Dileptons as Pre-equilibrium Probes

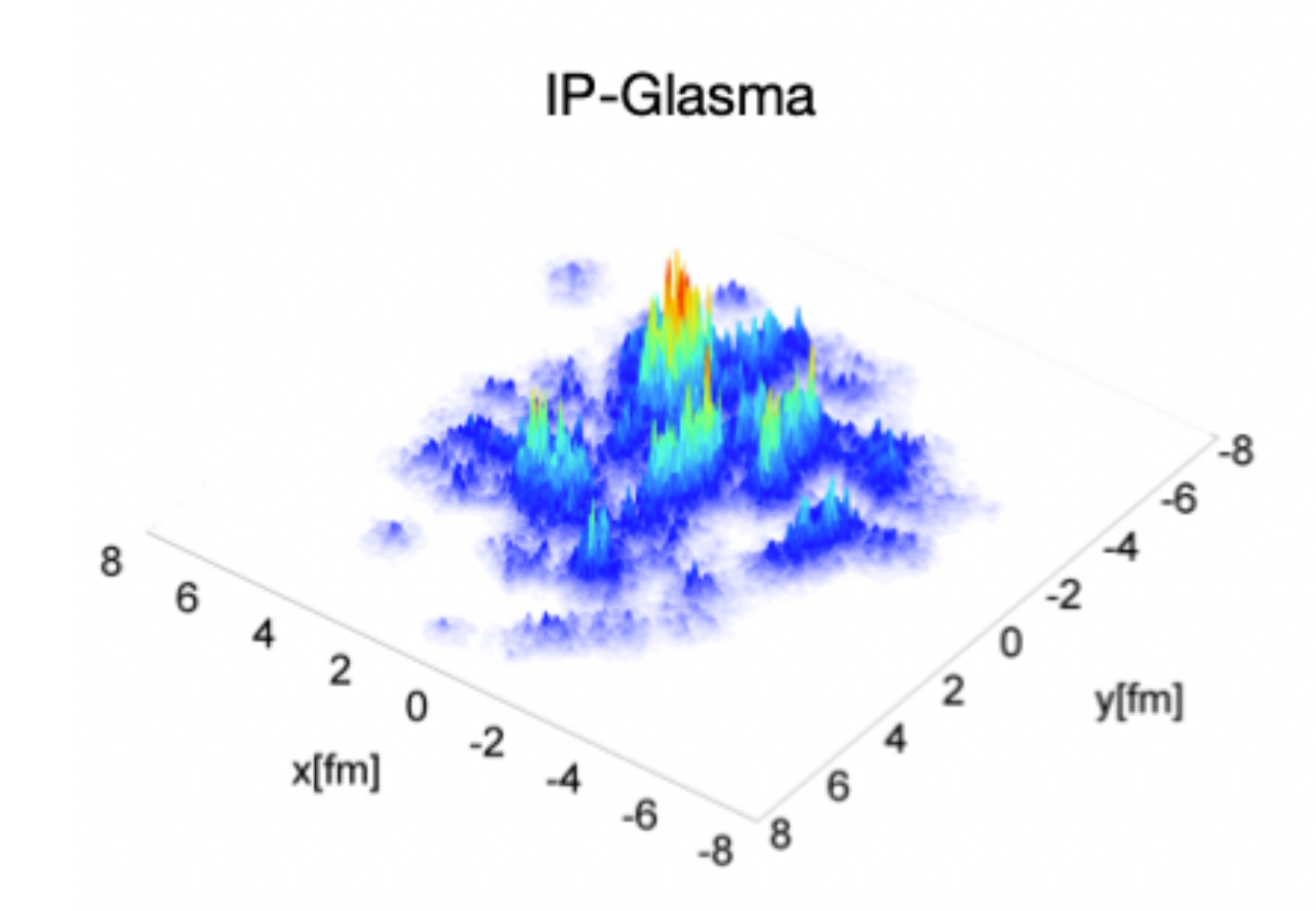


- Emitted throughout the evolution, carrying information about its local production point.
- Invariant mass M: frame-independent and not affected by blue-shift.
- Mass windows correspond to different stages/sources:
 - LMR: Decays of light mesons.
 - IMR: Thermal dileptons and decays of open heavy flavor.
 - HMR: Drell-Yan process and quarkonium decays.

 $\tau = 0^+ \text{ fm}$

Initial condition: IP-Glasma

- Color glass condensates.
- Evolved by Yang-Mills equations.



[Schenke, Tribedy & Venugopalan, PRL 108, 252301 (2012)] [Schenke, Tribedy & Venugopalan, PRC 86, 034908 (2012)]

 $\tau = 0^+ \text{ fm}$

Initial condition: IP-Glasma

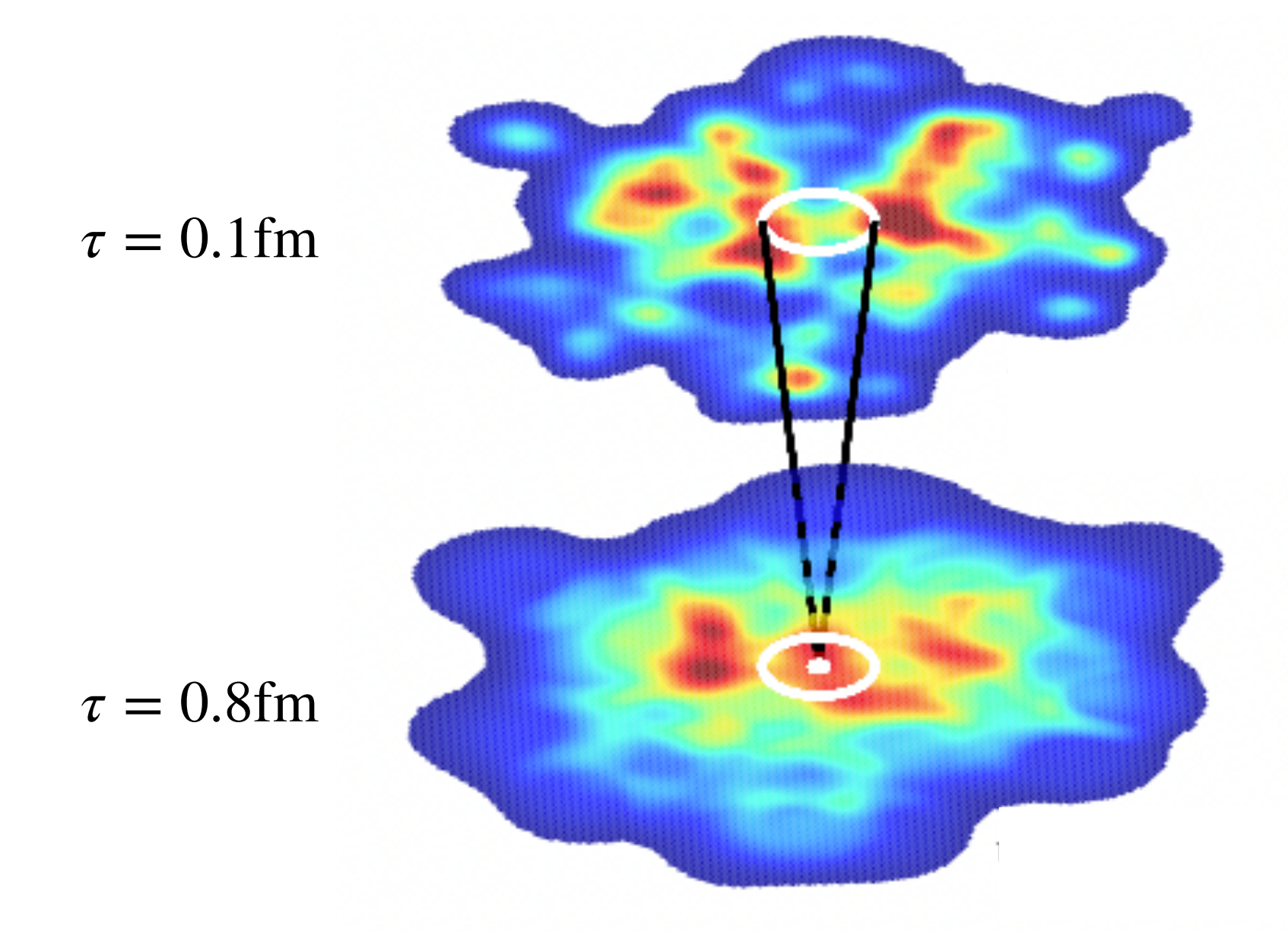
- Color glass condensates.
- Evolved by Yang-Mills equations.

 $\tau = 0.1 \text{ fm}$

Pre-equilibrium stage: KøMPøST

$$T^{\mu\nu}(\tau, \mathbf{x}) = \bar{T}^{\mu\nu}(\tau, \mathbf{x}) + \delta T^{\mu\nu}(\tau, \mathbf{x})$$

- Background and perturbation.
- Kinetic theory scaling curve and linear response.



[Kurkela, Mazeliauskas, Paquet, Schlichting & Teaney, PRC 99, 034910 (2019)] [Kurkela, Mazeliauskas, Paquet, Schlichting & Teaney, PRL122, 122302 (2019)]

 $\tau = 0^+ \text{ fm}$

Initial condition: IP-Glasma

- Color glass condensates.
- Evolved by Yang-Mills equations.

 $\tau = 0.1 \text{ fm}$

Pre-equilibrium stage: KøMPøST

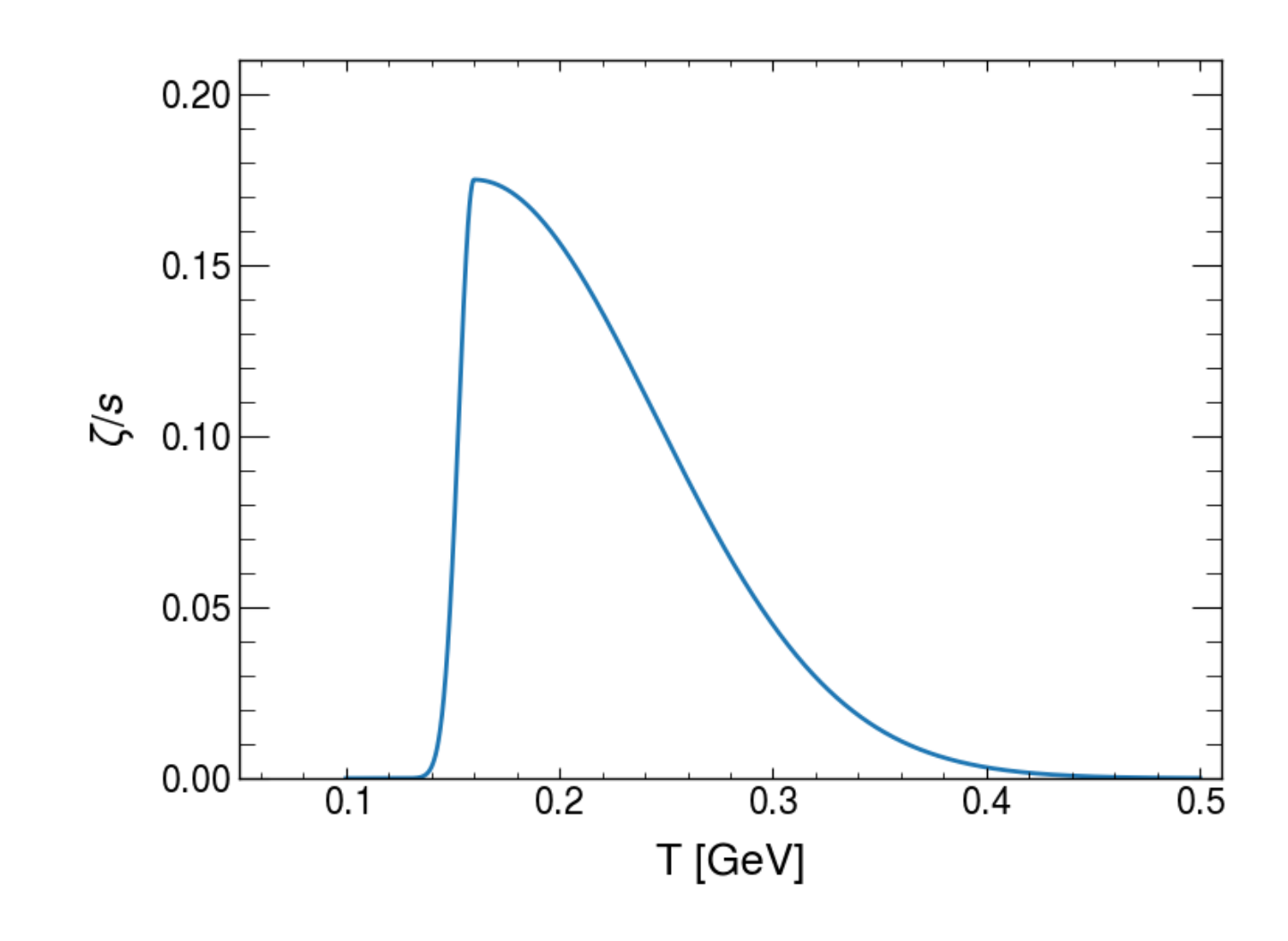
- Background and perturbations.
- Kinetic theory scaling curve and linear response.

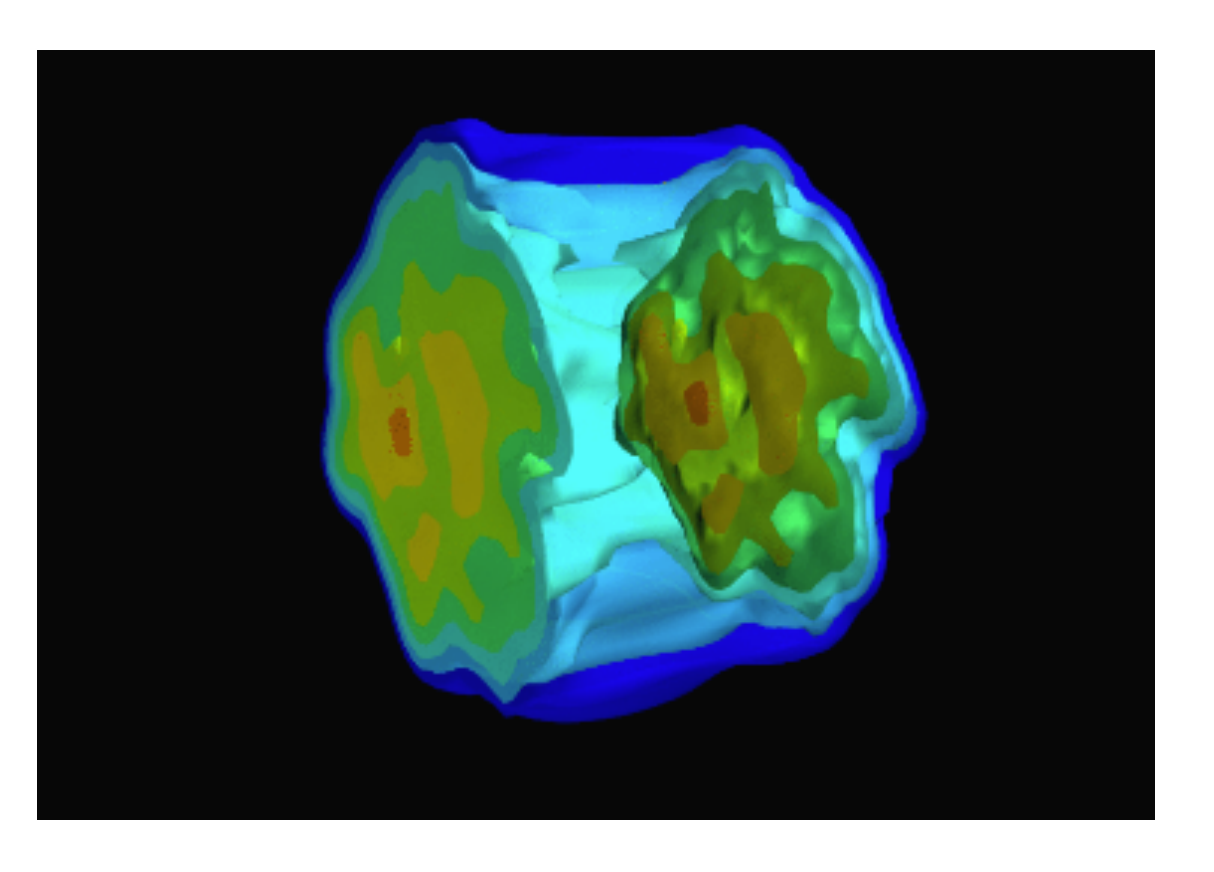
 $\tau = 0.8 \text{ fm}$

Hydrodynamic evolution: MUSIC

- (2+1)-D event-by-event 2nd viscous hydrodynamics model.
- Shear viscosity $\eta/s = 0.12$ and bulk viscosity $\zeta/s(T)$.
- HotQCD+hadron gas equation of states.

 $\tau \approx 10 \text{ fm}$





[Paquet, Shen, Denicol, Luzum, Schenke, Jeon & Gale, PRC 93, 044906 (2016)] [Schenke, Jeon & Gale, PRC 82, 014903 (2010)] [Schenke, Jeon & Gale, PRL 106, 042301 (2011)] [Gale, Paquet, Schenke & Shen, PRC 105, 014909 (2022)]

 $\tau = 0^+ \text{ fm}$

Initial condition: IP-Glasma

- Color glass condensates.
- Evolved by Yang-Mills equations.

 $\tau = 0.1 \text{ fm}$

Pre-equilibrium stage: KøMPøST

- Background and perturbations.
- Kinetic theory scaling curve and linear response.

 $\tau = 0.8 \text{ fm}$

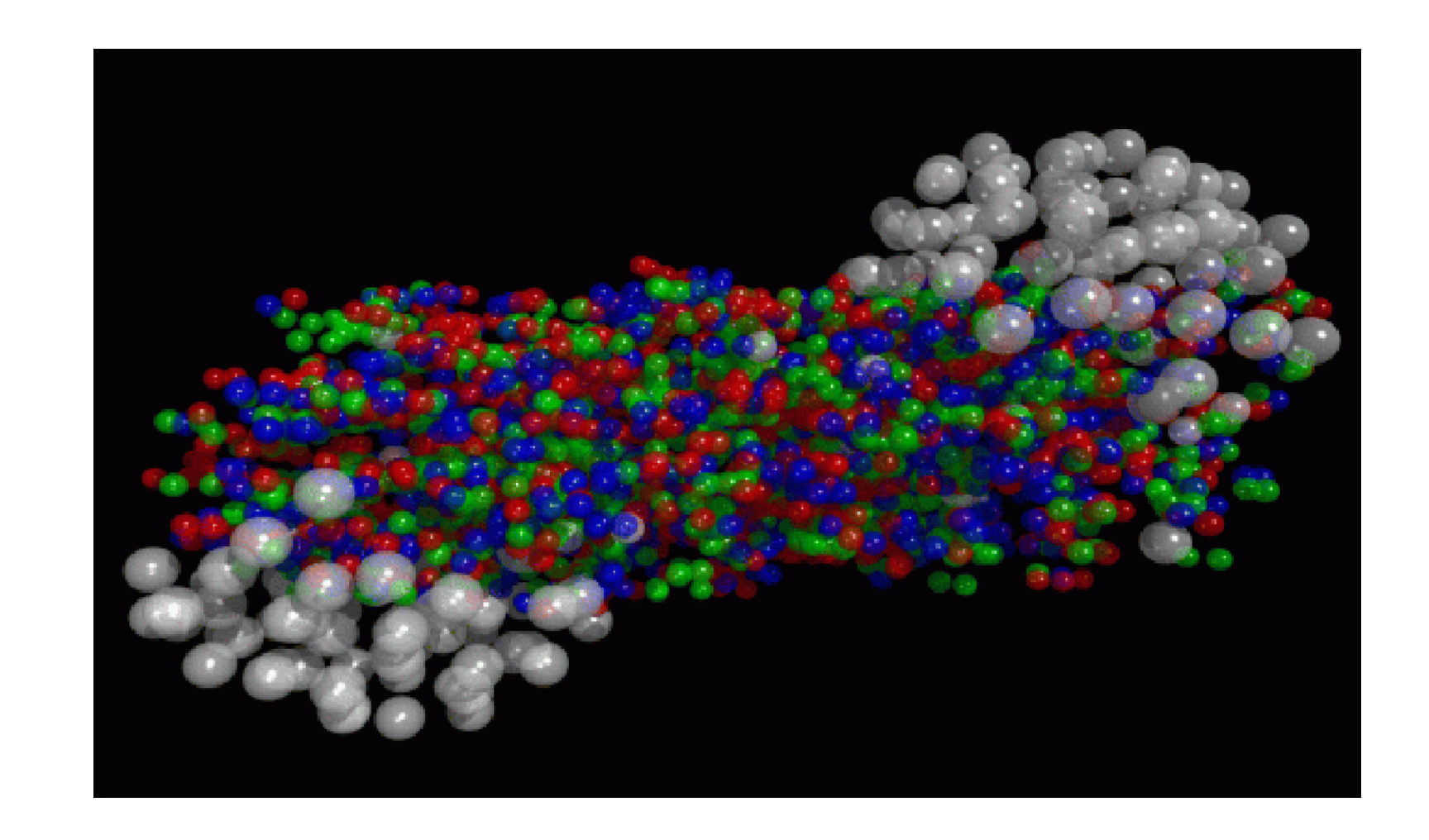
Hydrodynamic evolution: MUSIC

- (2+1)-D event-by-event 2nd viscous hydrodynamics model.
- Shear viscosity $\eta/s = 0.12$ and bulk viscosity $\zeta/s(T)$.
- HotQCD+hadron gas equation of states.

 $\tau \approx 10 \text{ fm}$

Hadronic cascade: URQMD

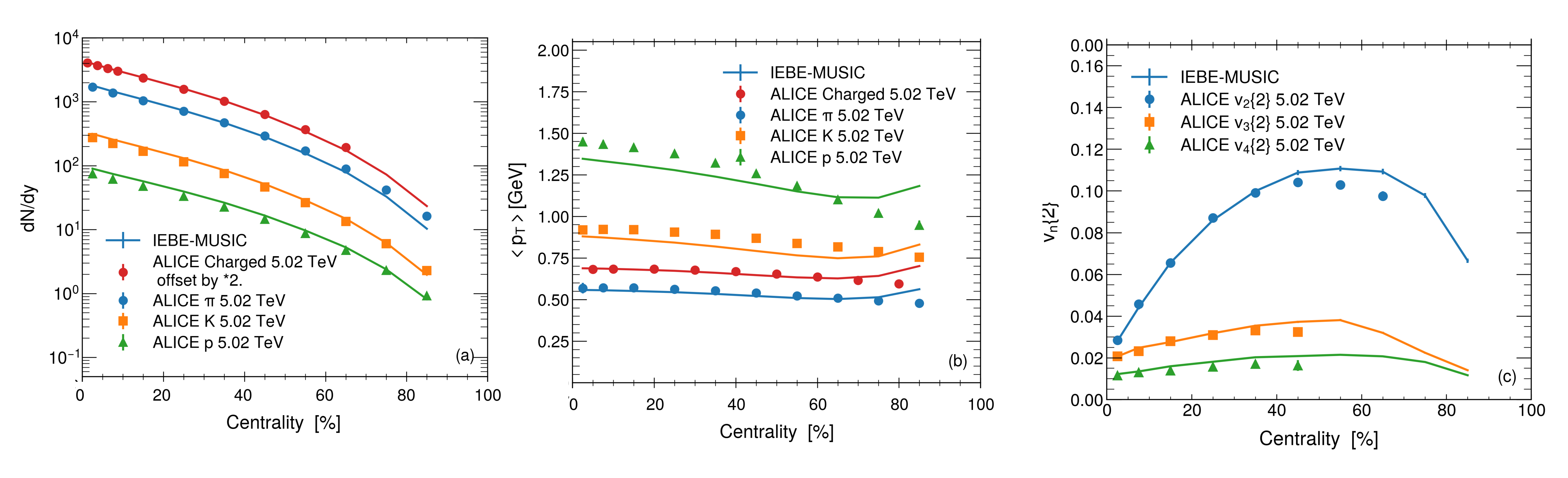
- Elastic collisions.
- Resonance formation and decays.



[S. A. Bass et al, Prog. Part. Nucl. Phys. 41, 255–369 (1998)]

Model Calibration

[X.Y. Wu, L. Du, C. Gale and S. Jeon, Phys.Rev.C 110 (2024) 5, 054904]



- Hydrodynamic results agree well with hadron multiplicity in all centrality bins.
- Small discrepancy in mean transverse momentum $\langle p_T \rangle$ and anisotropic flow $v_n\{2\}$ originates from vanishing bulk viscosity in IP-Glasma and KøMPøST.
- The discrepancy increases in peripheral collision due to shorter lifetime in hydrodynamic phase.

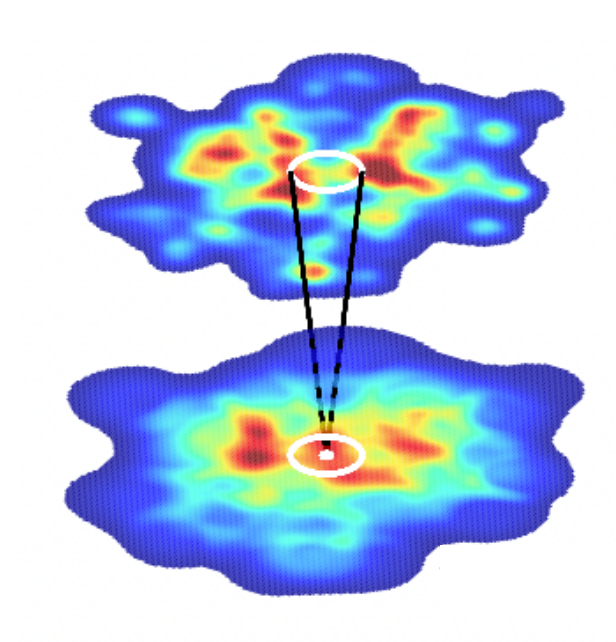
Dilepton Sources

 $\tau = 0^+ \text{ fm}$

Initial condition: IP-Glasma

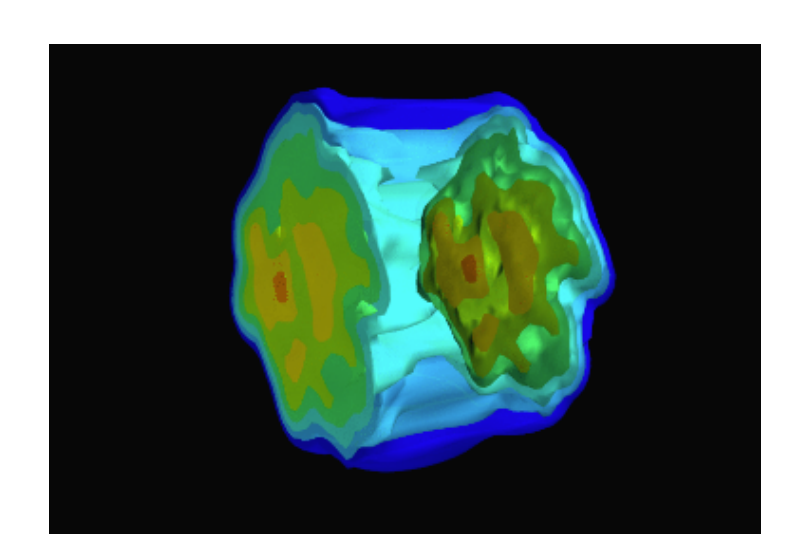
 $\tau = 0.1 \text{ fm}$

Pre-equilibrium stage: KøMPøST



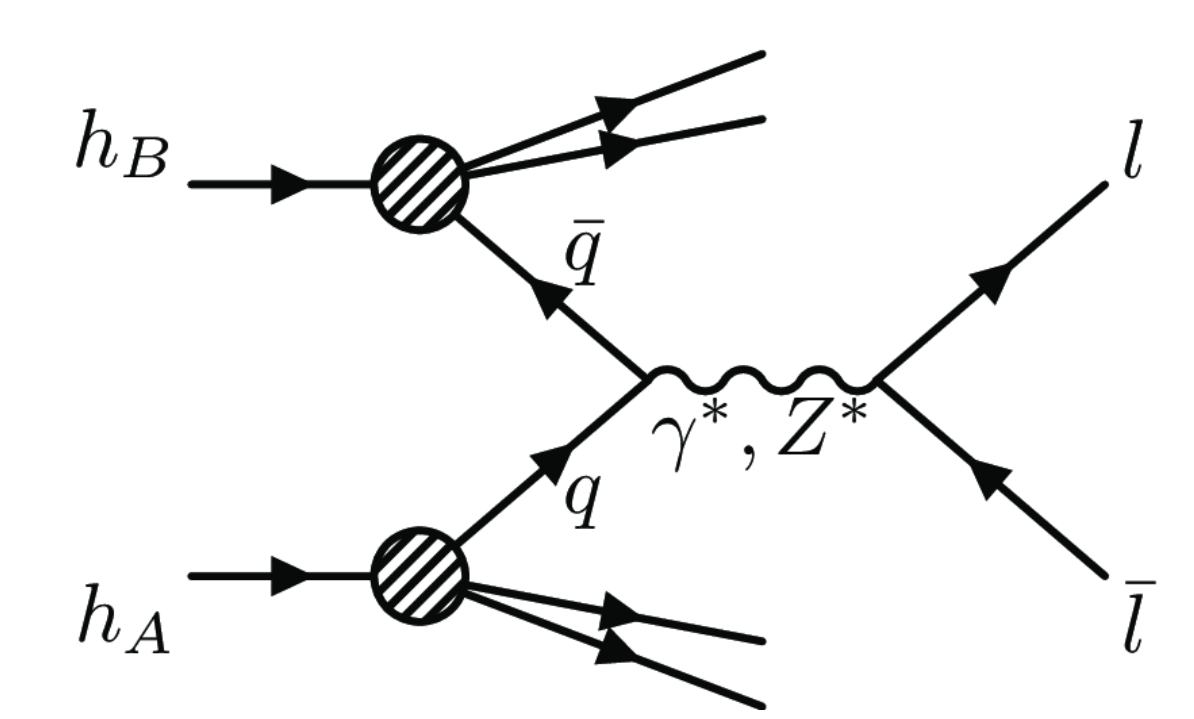
 $\tau = 0.8 \text{ fm}$

Hydrodynamic evolution: MUSIC



 $\tau \approx 10 \text{ fm}$

Hadronic cascade: URQMD



Drell-Yan dilepton

DYTurbo package: NLO order in p+p collision.

In A+A collisions

$$\frac{dN_{ee}^{DY}}{dMdy} = \frac{d\sigma_{ee}^{DY;pp}}{dMdy} \cdot \frac{N_{col}}{\sigma_{in}^{pp}}$$

nPDF: EPPS16nlo-CT14nlo-Pb208.

Thickness function: MC-Glauber.

[Camarda et al., EPJC 80, 251 (2020)] [Eskola, Paakkinen, Paukkunen & Salgado, EPJC 77, 163 (2017)] [Loizides, Kamin & Enterria, PRC 97, 054910 (2018)]

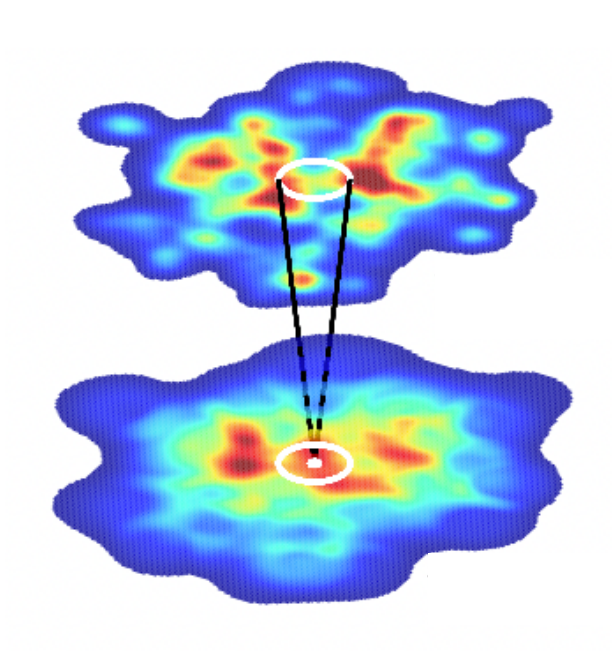
Dilepton Sources

 $\tau = 0^+ \text{ fm}$

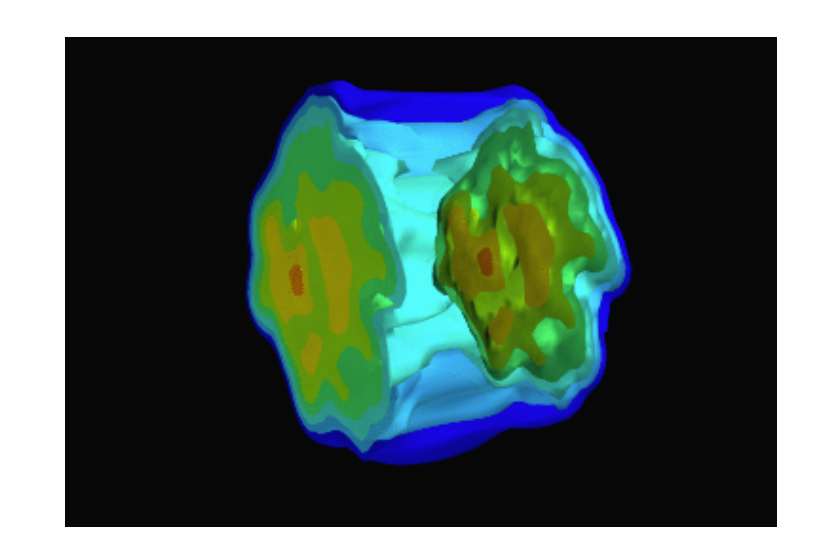
 $\tau = 0.1 \text{ fm}$

Initial condition: IP-Glasma

Pre-equilibrium stage: KøMPøST



 $\tau = 0.8 \text{ fm}$ Hydrodynamic evolution: MUSIC



 $\tau \approx 10 \text{ fm}$ Hadronic cascade: URQMD

Drell-Yan dilepton

Thermal dilepton

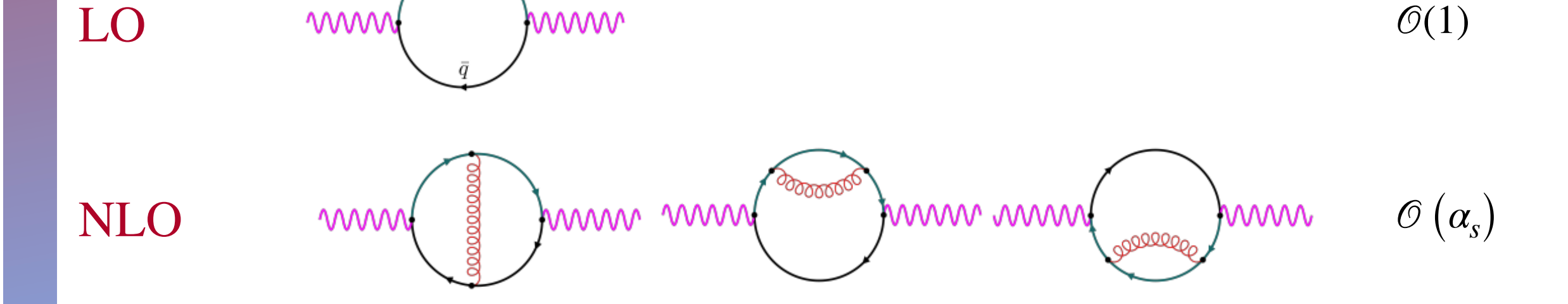
 $T(x), U^{\mu}(x)$

 $T(x), U^{\mu}(x)$

$$\frac{dN_{l\bar{l}}}{MdMdy'} = \int d^4x p_T' dp_T' d\phi' \frac{d\Gamma_{l\bar{l}}}{d^4P} \bigg|_{P^{\mu} = \Lambda^{\nu}_{\mu}(U(X))P}$$

$$\frac{dN_{l\bar{l}}}{p_T' dp_T' dy'} = \int d^4x M dM d\phi' \frac{d\Gamma_{l\bar{l}}}{d^4P} \bigg|_{P^{\mu} = \Lambda^{\nu}_{\mu}(U(X))P'}$$

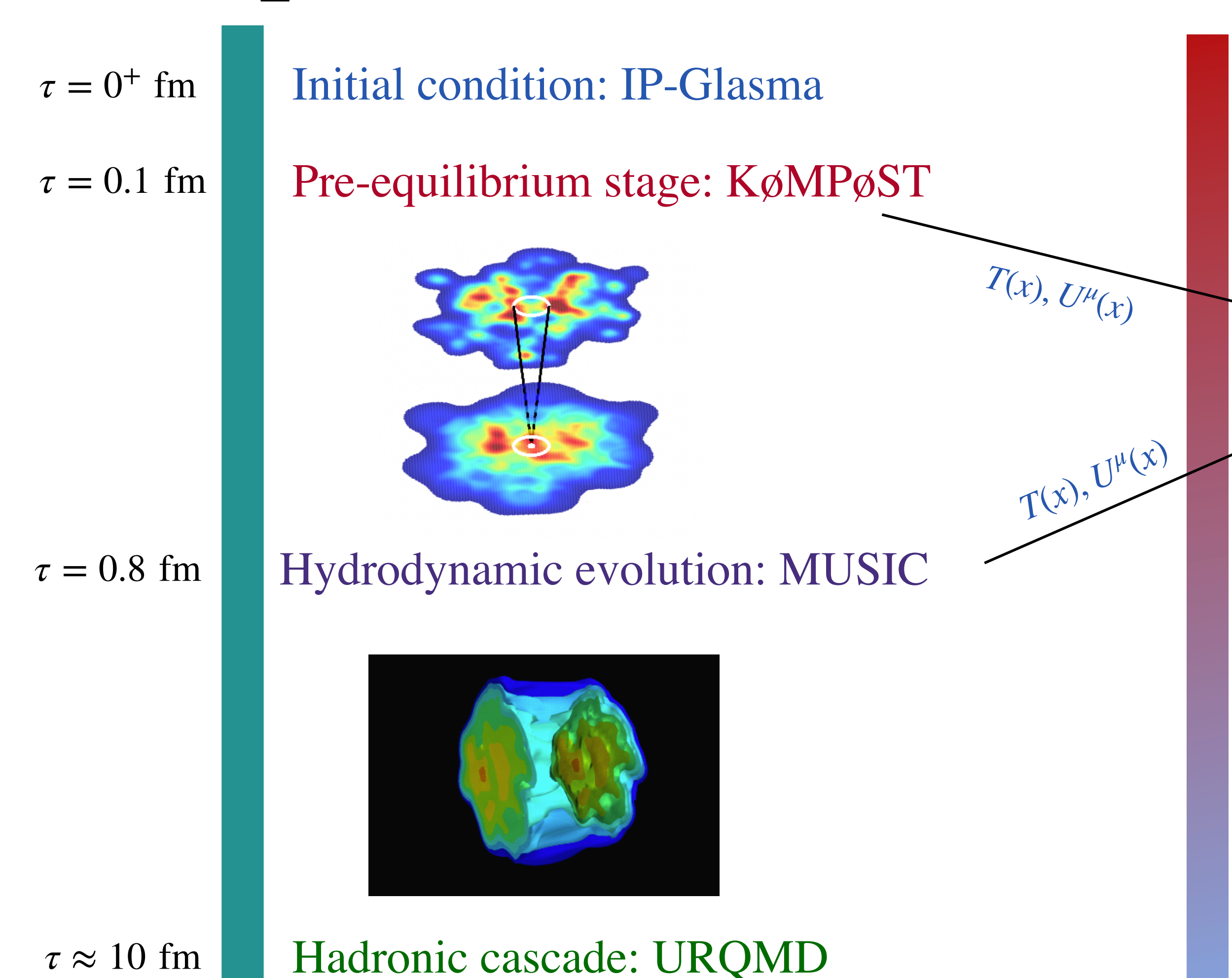
 $\frac{d\mathbf{1}_{l\bar{l}}}{d^4P}$: the differential dileption emission rate at NLO with finite μ_B .



 $\mathcal{O}\left(\alpha_s^i\right), \quad i \geq 2$

[Churchill, Du, Gale, Jackson & Jeon, PRC 109, 044915 (2024), PRL 132, 172301 (2024)]

Dilepton Sources



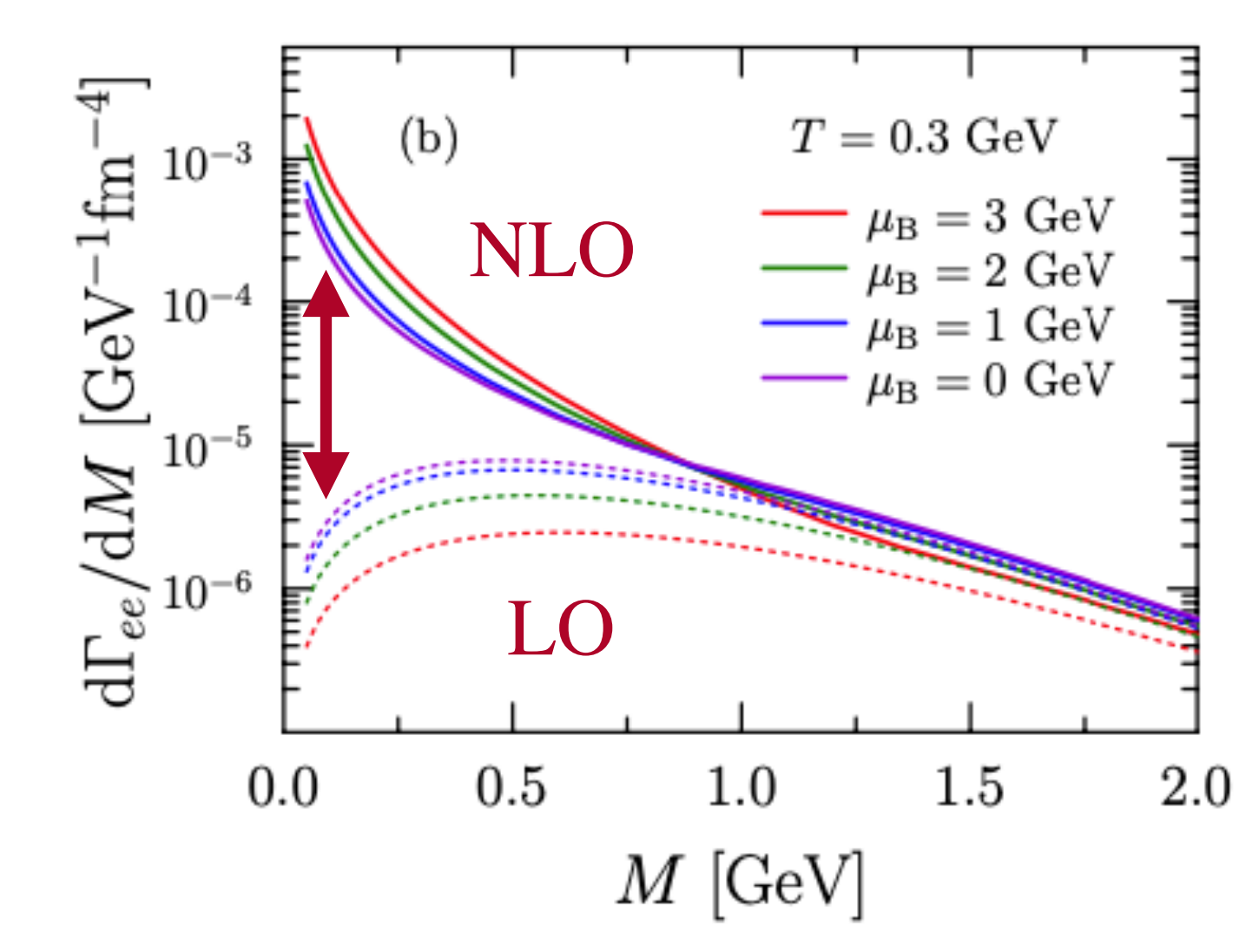
Drell-Yan dilepton

Thermal dilepton

$$\frac{dN_{l\bar{l}}}{MdMdy'} = \int d^4x p_T' dp_T' d\phi' \frac{d\Gamma_{l\bar{l}}}{d^4P} \bigg|_{P^{\mu} = \Lambda^{\nu}_{\mu}(U(X))P'^{\mu}}$$

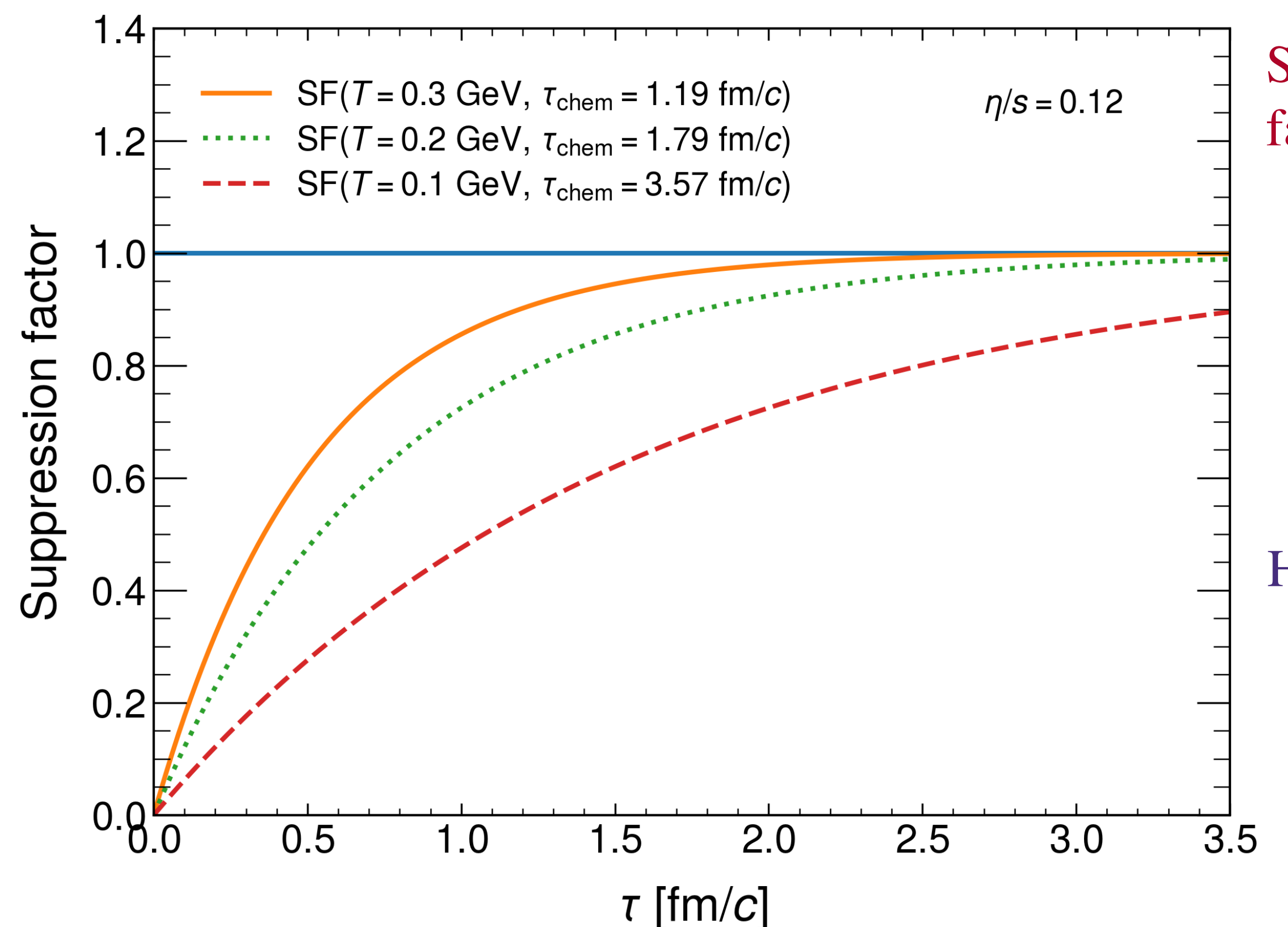
$$\frac{dN_{l\bar{l}}}{p_T' dp_T' dy'} = \int d^4x MdMd\phi' \frac{d\Gamma_{l\bar{l}}}{d^4P} \bigg|_{P^{\mu} = \Lambda^{\nu}(U(X))P''}$$

 $\frac{d\Gamma_{l\bar{l}}}{d^4P}$: the differential dilepton emission rate at NLO with finite μ_B .



Chemical Equilibrium

- The gluon fields dominate in the early stage.
- Quarks and anti-quarks are produced via $gg \to q\bar{q}$ and $g \to q\bar{q}$.
- The effective suppression factor $SF(T,\tau)$ is introduced in relation to chemical relaxation time $\tau_R = 4\pi\eta/Ts$.

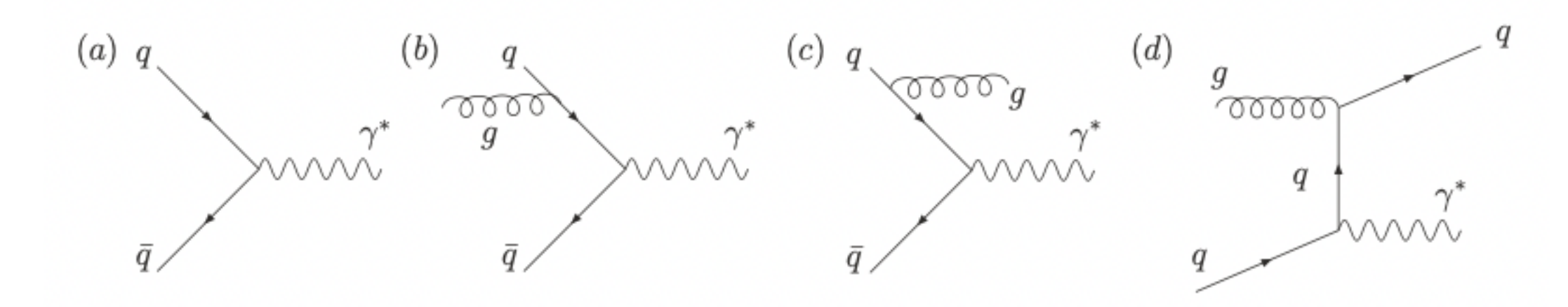


Systems with higher temperatures reach chemical equilibrium faster than those at lower temperatures.

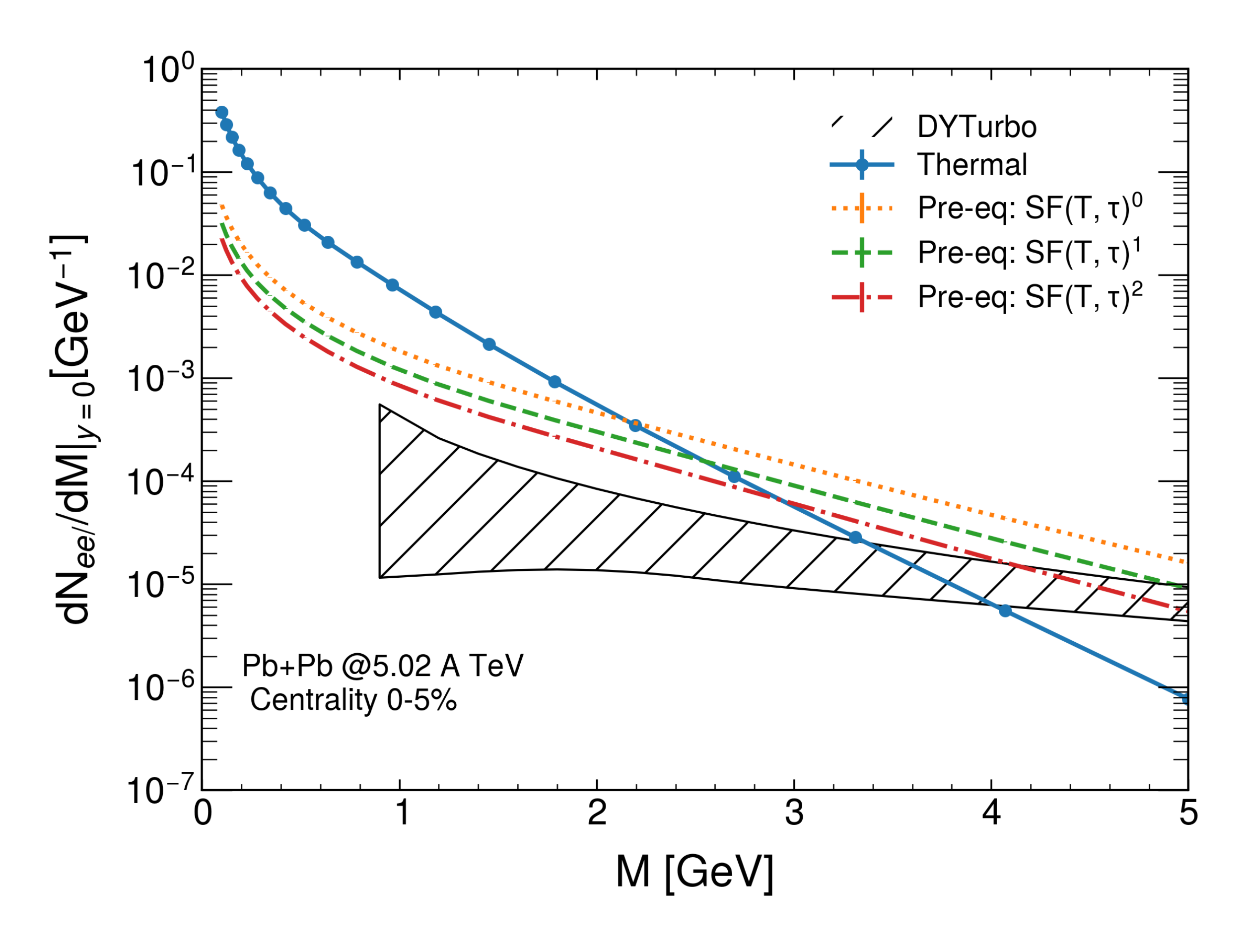
$$\frac{dN_{l\bar{l}}}{MdMdy'} = \int dV \operatorname{SF}(T, \tau)^{n} \frac{d\Gamma_{l\bar{l}}}{d^{4}P} \bigg|_{P^{\mu} = \Lambda_{\mu}^{\nu}(U(X))P'^{\nu}} p_{T}' dp_{T}' d\phi'$$

$$\frac{dN_{l\bar{l}}}{p_{T}' dp_{T}' dy'} = \int dV \operatorname{SF}(T, \tau)^{n} \frac{d\Gamma_{l\bar{l}}}{d^{4}P} \bigg|_{P^{\mu} = \Lambda_{\mu}^{\nu}(U(X))P''} MdMd\phi'$$

Here n = 0,1,2.

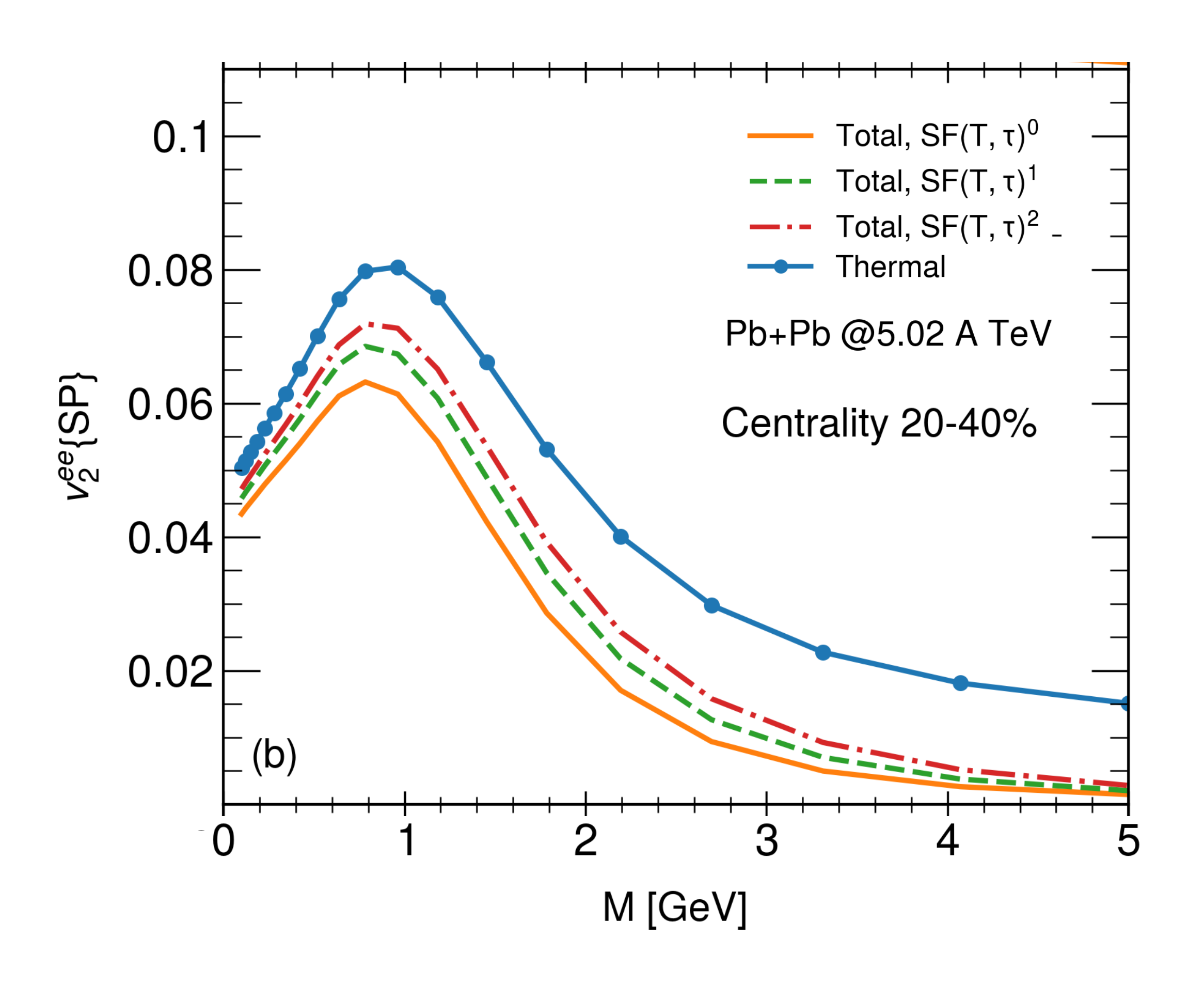


Dilepton M spectrum



- Thermal dilepton production dominates in the LMR.
- The pre-equilibrium dileptons are the dominant source over thermal dileptons in the IMR.
- Drell-Yan dileptons are consistently smaller than the preequilibrium contribution until the HMR.
- Dilepton production during the pre-equilibrium phase will be sensitive to the power of suppression factor for chemical equilibrium.

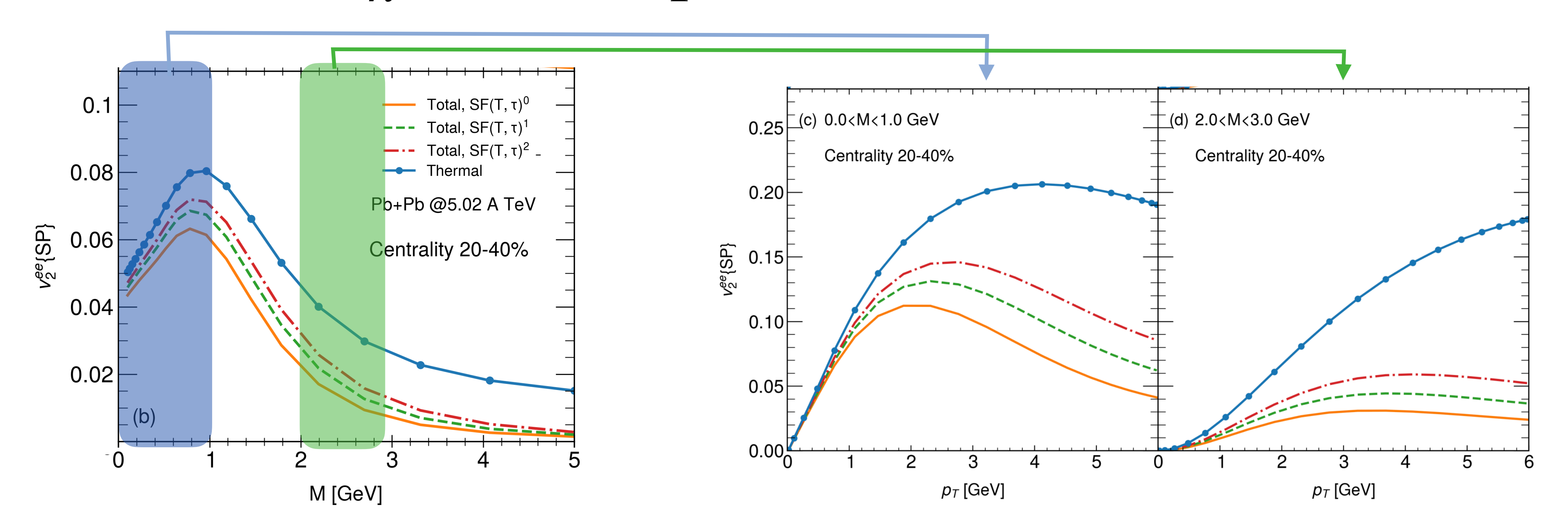
Dilepton $v_n^{ee}\{SP\}(M)$



• The scalar-product (SP) method:

$$v_n^{l\bar{l}}\{\mathrm{SP}\}(X) = \frac{\left\langle v_n^{l\bar{l}}(X)v_n^h\cos\left\{n\left[\Psi_n^{l\bar{l}}(X) - \Psi_n^h\right]\right\}\right\rangle}{\sqrt{\left\langle \left(v_n^h\right)^2\right\rangle}}$$

- The total $v_2^{ee}(M)$ will be suppressed due to the almost zero momentum anisotropy in the pre-equilibrium stage.
- For the higher order of the suppression factor, the total dilepton flow $v_2^{ee}(M)$ moves closer to that of thermal dileptons.



- Total elliptic flow $v_2^{ee}(p_T)$ is highly sensitive to the effects of chemical equilibrium.
- 0 < M < 1 GeV:
 - after considering the pre-equilibrium stage, the total dilepton flow $v_2^{ee}(p_T)$ is significantly suppressed.
- 2 < M < 3 GeV:
 - the total dilepton elliptic flow $v_2^{ee}(p_T)$ shows a noticeable reduction compared to that in the LMR.

Outline

- Introduction
- Dileptons in the Pre-equilibrium Stage
- Dilepton polarization
- Dilepton and photons at RHIC-BES
- Summary

Dilepton polarization

• The dilepton production rate:

$$\frac{dR_{l\bar{l}}}{d^4K} \propto \rho_L + 2\rho_T$$

What is
$$\rho_T - \rho_L$$
?

• The angular distribution of leptons in the virtual photon's rest frame:

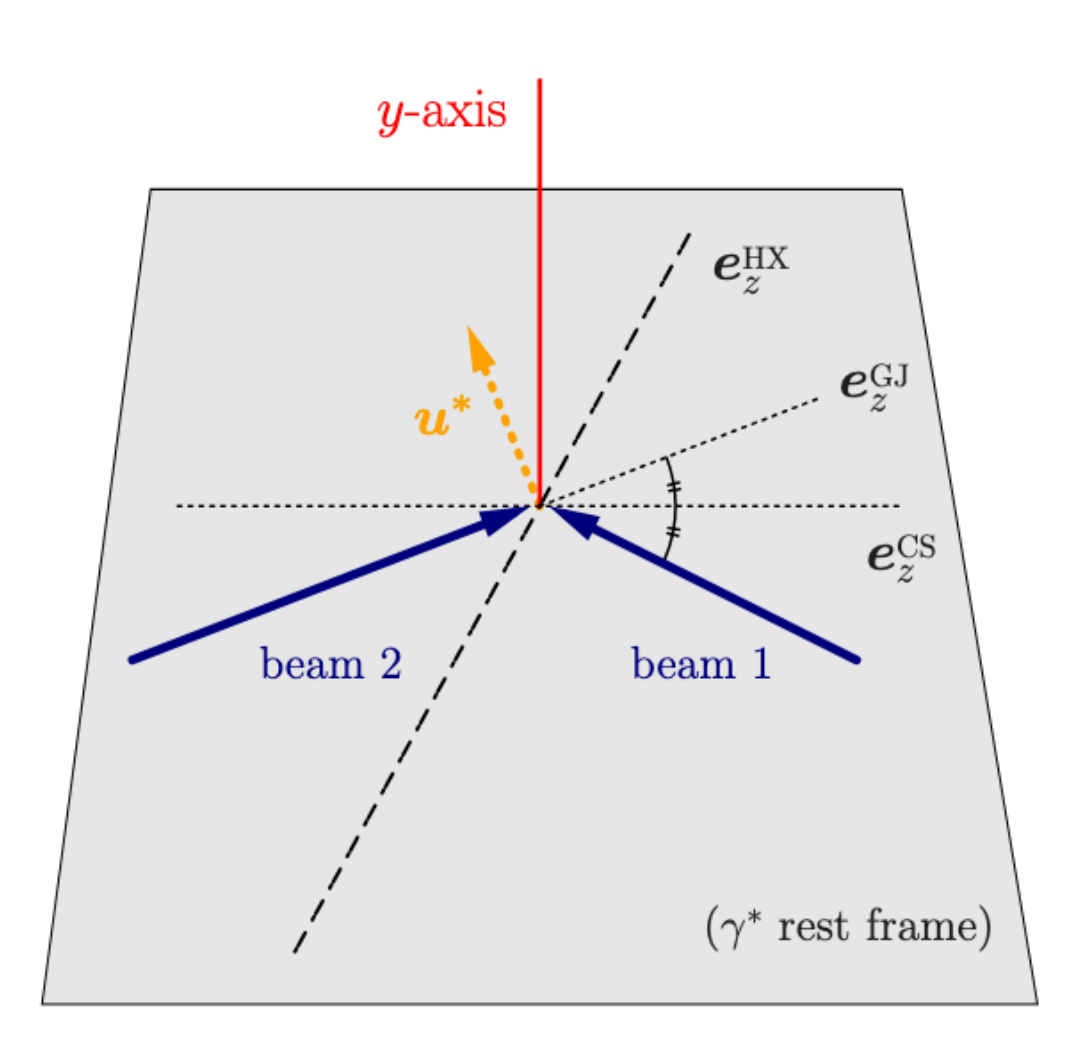
$$\frac{dN}{d^4K d\Omega_{\ell}} = \mathcal{N} \left(1 + \frac{\lambda_{\theta}}{l} \cos^2 \theta_{\ell} + \frac{\lambda_{\phi}}{l} \sin^2 \theta_{\ell} \cos 2\phi_{\ell} + \frac{\lambda_{\theta\phi}}{l} \sin 2\theta_{\ell} \cos \phi_{\ell} + \frac{\lambda_{\phi}^{\perp}}{l} \sin^2 \theta_{\ell} \sin 2\phi_{\ell} + \frac{\lambda_{\phi}^{\perp}}{l} \sin 2\theta_{\ell} \sin 2\phi_{\ell} + \frac{\lambda_{\phi}^{\perp}}{l} \sin 2\phi_{\ell} \sin 2\phi_{\ell} \sin 2\phi_{\ell} \sin 2\phi_{\ell} \sin 2\phi_{\ell} + \frac{\lambda_{\phi}^{\perp}}{l} \sin 2\phi_{\ell} \sin 2\phi_{$$

• Polarization parameters λ_* are frame-dependent.

Helicity (HX): direction of the virtual photon momentum.

Z-axis Collins-Soper (CS): bisector of the angle between the two beam momenta.

Gottfried-Jackson (GJ): direction of one of the colliding beam momenta.



Dilepton polarization

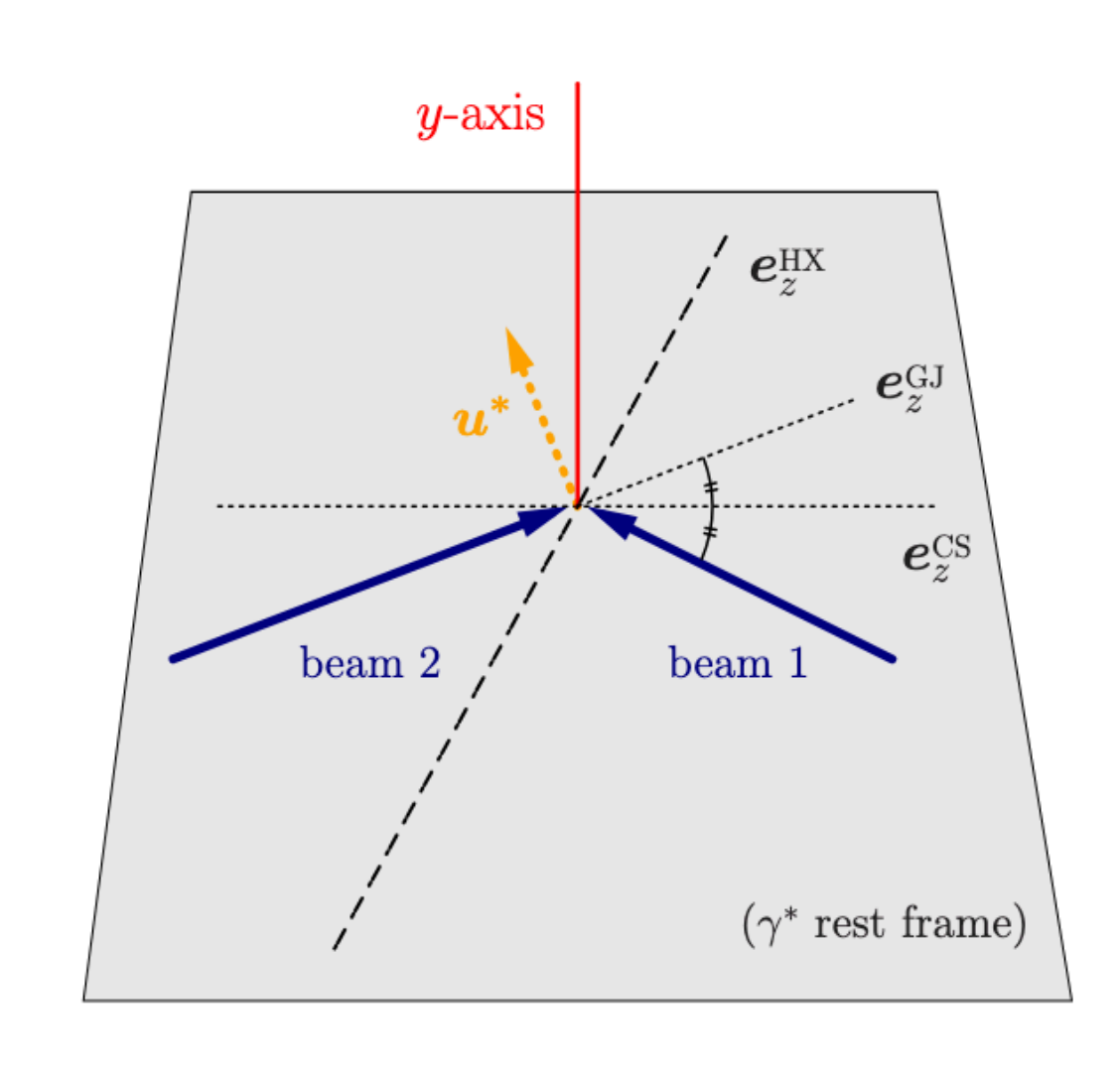
- $\frac{dR_{l\bar{l}}}{d^4K} \propto \rho_L + 2\rho_T$ • The dilepton production rate:
- The angular distribution of leptons in the virtual photon's rest frame:

$$\frac{dN}{d^4K d\Omega_{\ell}} = \mathcal{N} \left(1 + \frac{\lambda_{\theta}}{l} \cos^2 \theta_{\ell} + \frac{\lambda_{\phi}}{l} \sin^2 \theta_{\ell} \cos 2\phi_{\ell} + \frac{\lambda_{\theta\phi}}{l} \sin 2\theta_{\ell} \cos \phi_{\ell} + \frac{\lambda_{\phi}^{\perp}}{l} \sin^2 \theta_{\ell} \sin 2\phi_{\ell} + \frac{\lambda_{\phi}^{\perp}}{l} \sin 2\theta_{\ell} \sin 2\phi_{\ell} + \frac{\lambda_{\phi}^{\perp}}{l} \sin 2\phi_{\ell} \sin 2\phi_{$$

- Polarization parameters λ_* are frame-dependent.
- For a plasma at rest $u^{\mu} = (1,0)$ and at the HX-frame:

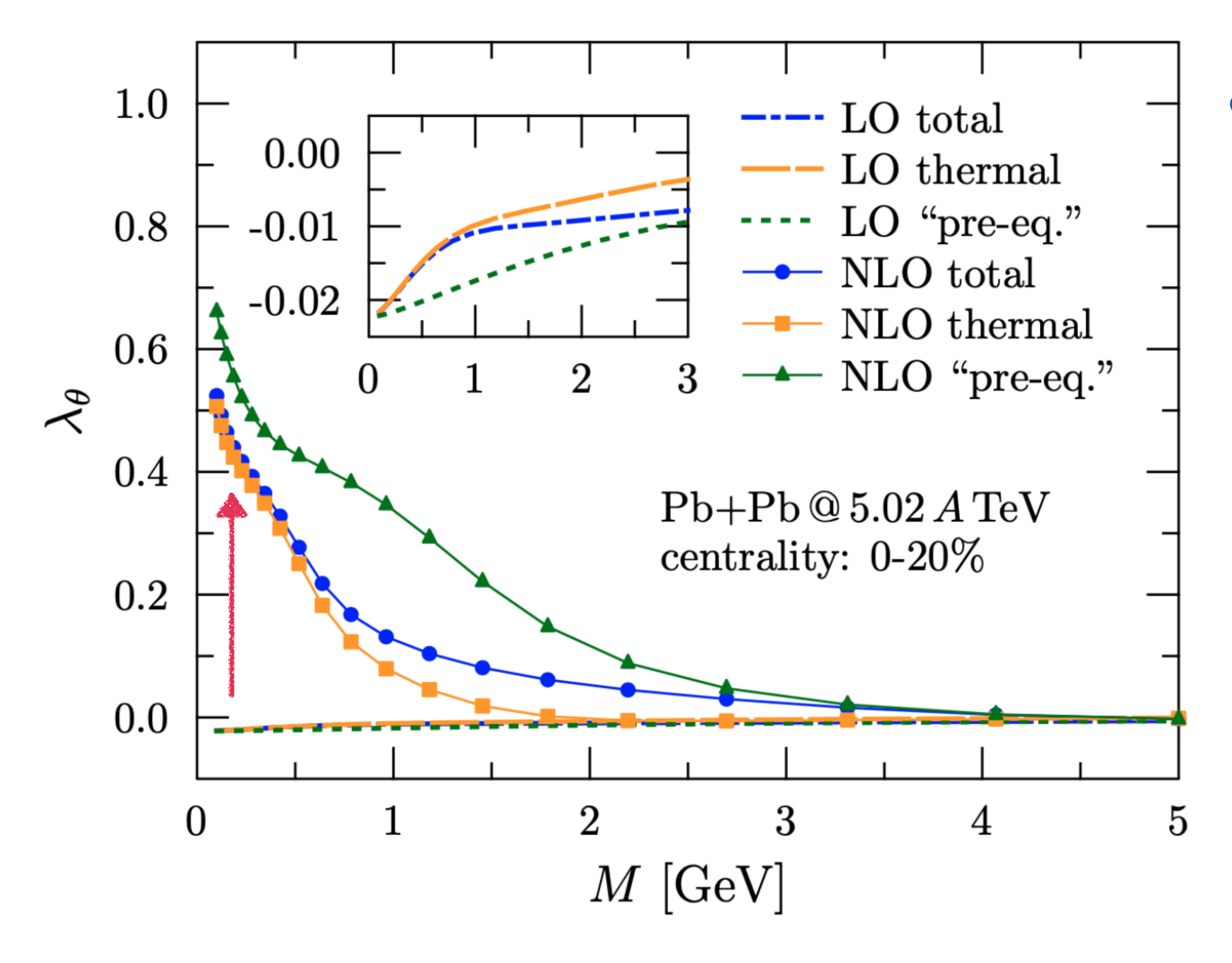
$$\lambda_{\theta} \simeq \frac{\rho_T - \rho_L}{\rho_T + \rho_L}$$
 with

 $\lambda_{\theta} \simeq \frac{\rho_T - \rho_L}{\rho_T + \rho_L}$ with $\begin{cases} \lambda_{\theta} = 1 & \text{transverse polarization} \\ \lambda_{\theta} = -1 & \text{longitudinal polarization} \\ \lambda_{\theta} = 0 & \text{unpolarized} \end{cases}$

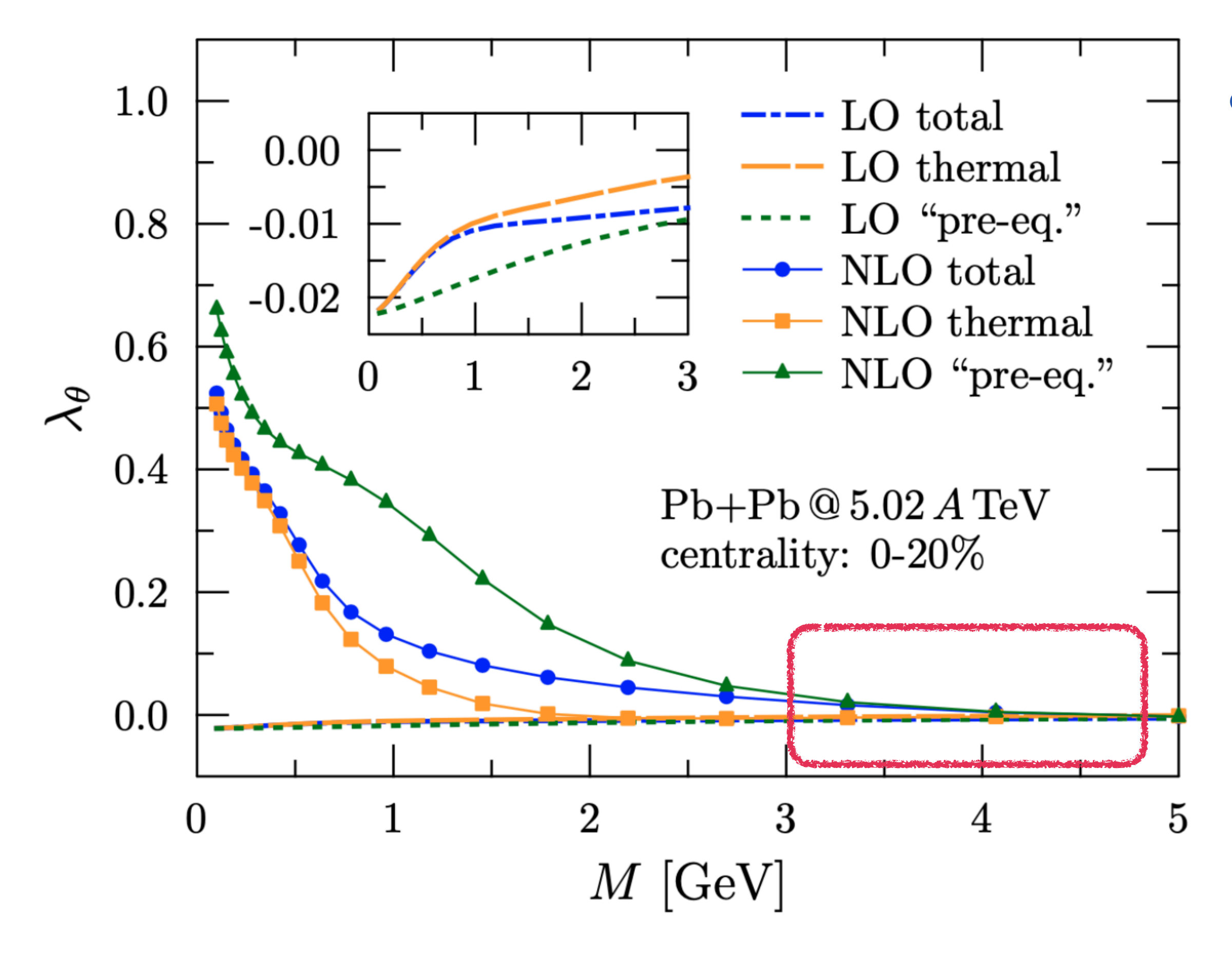


• The dilepton polarization provides another unique tool to study medium properties.

[Wu, Gao, Forster, Gale, Jackson and Jeon, PRL 134 (2025) 24, 242301]

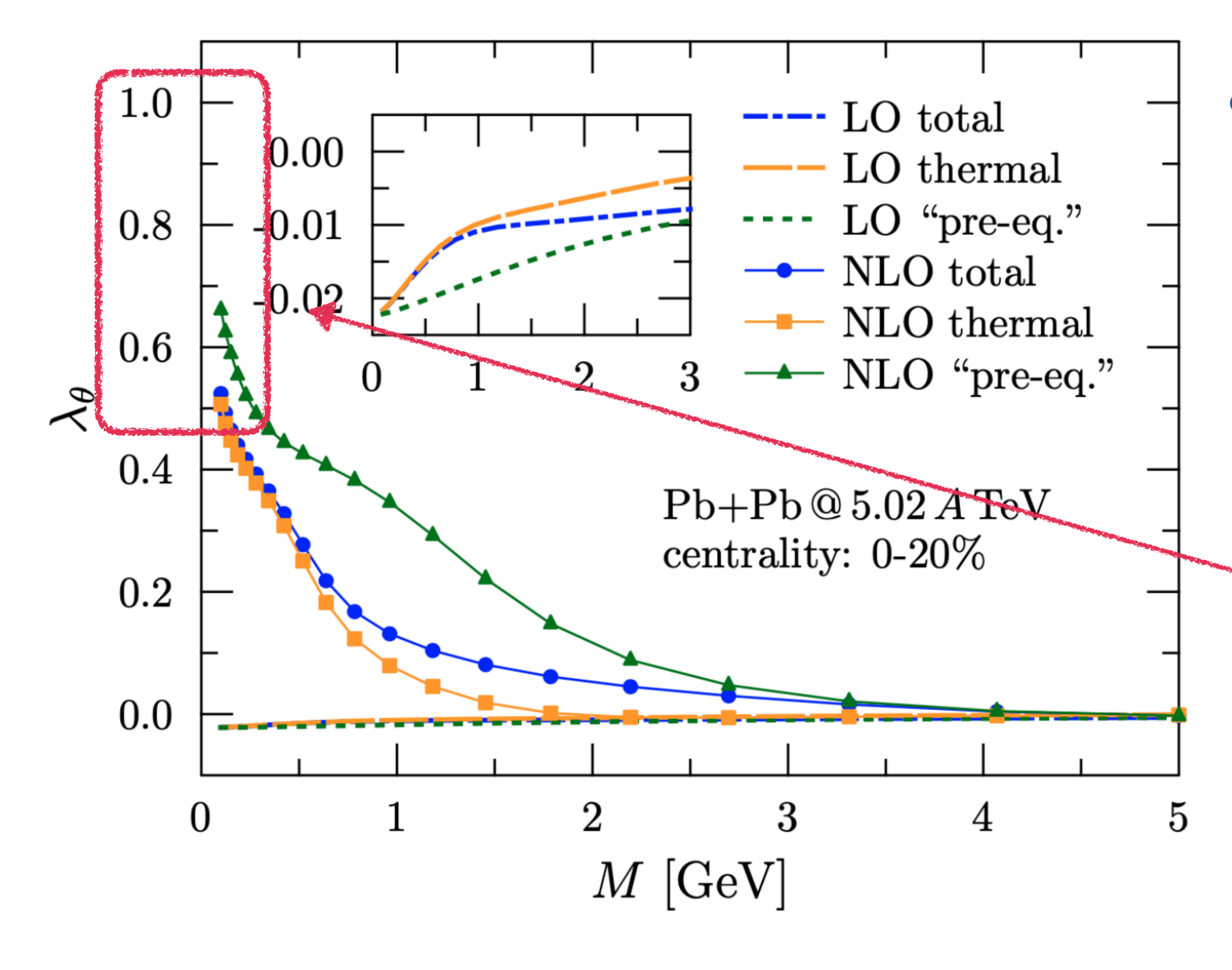


- NLO and LO results differ significantly.
 - $M \rightarrow 0$, the virtual photon behaves like a real photon, exhibiting only transverse polarization.

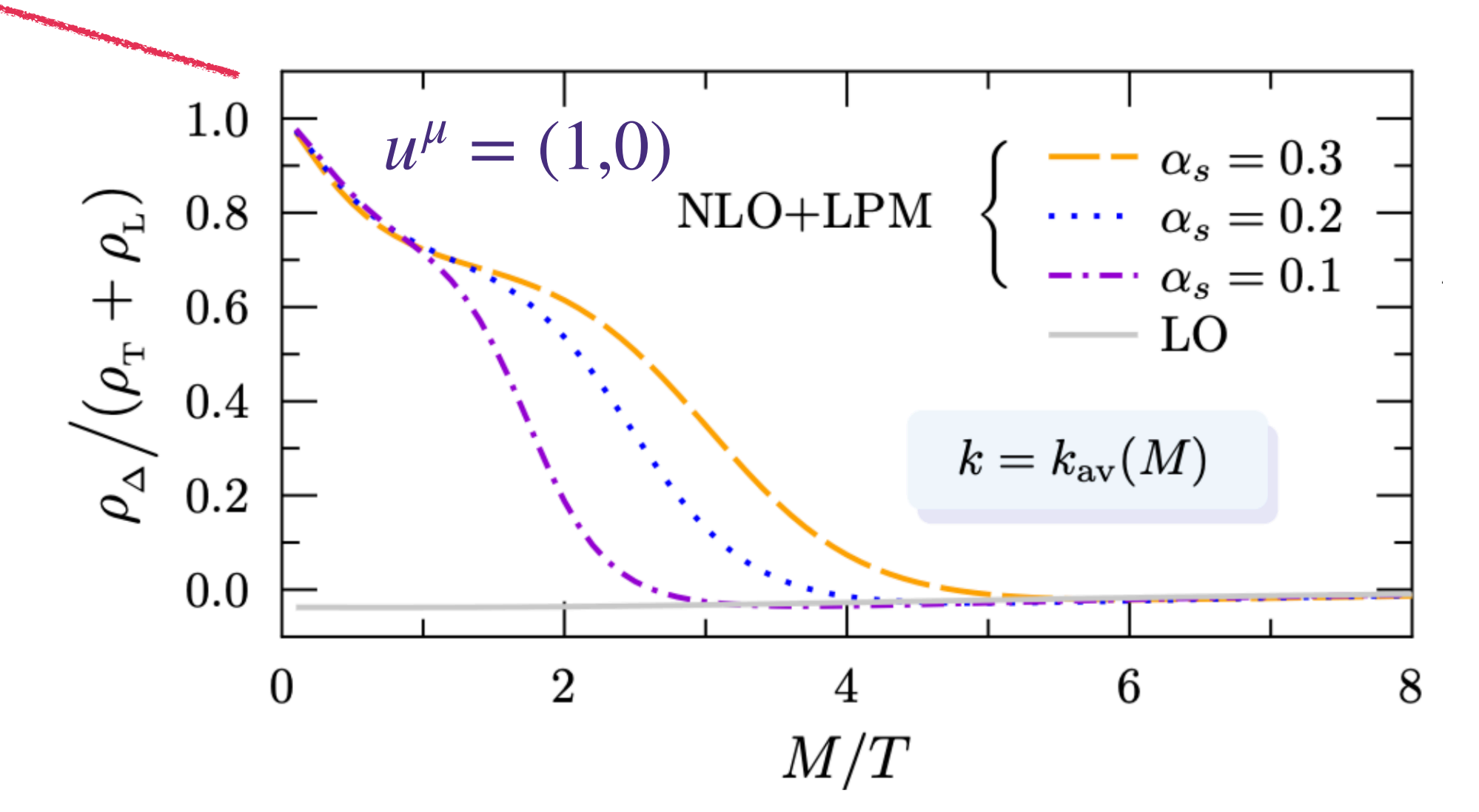


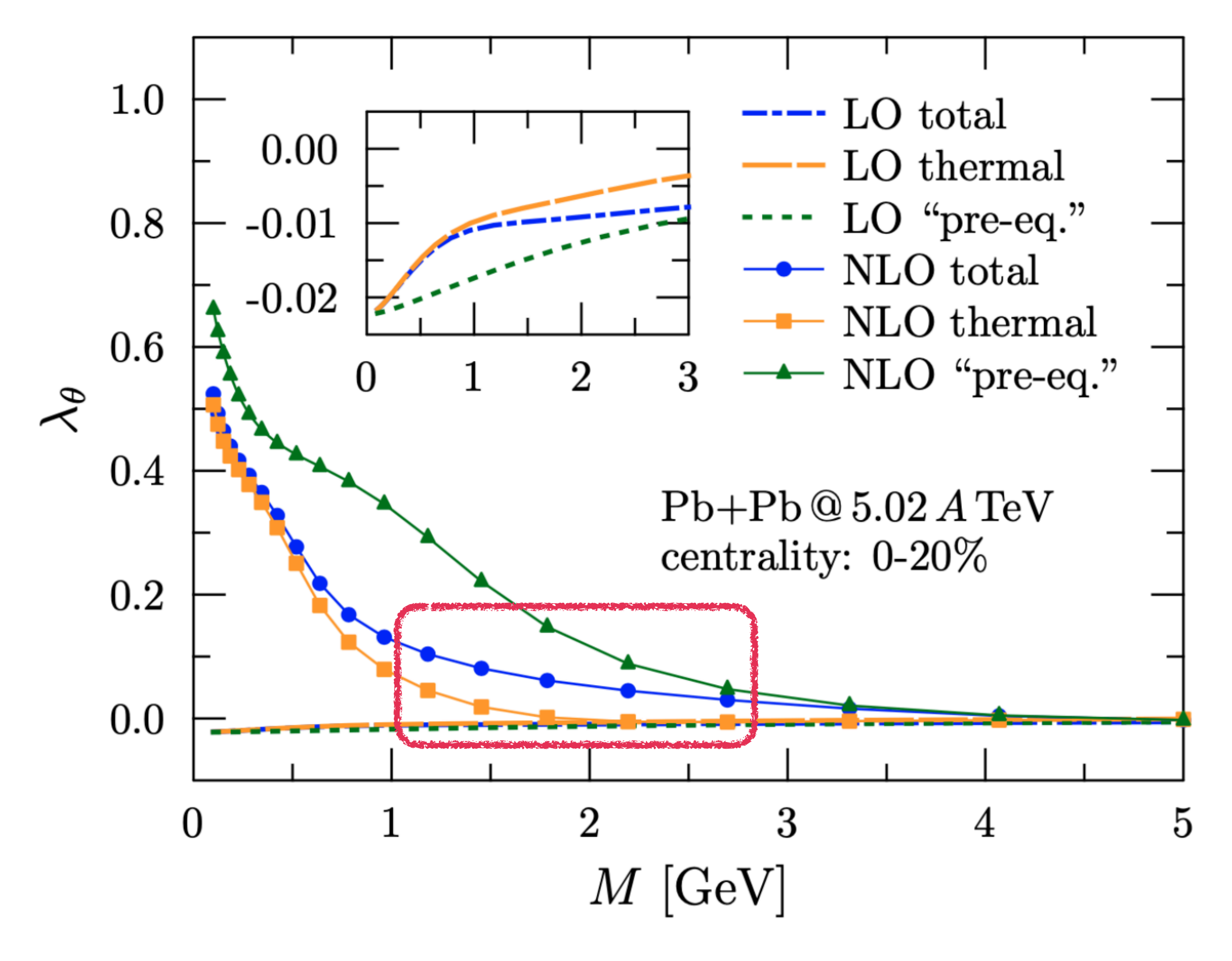
- NLO and LO results differ significantly.
 - $M \rightarrow 0$, the virtual photon behaves like a real photon, exhibiting only transverse polarization.
 - $M \to \infty$, both LO and NLO dilepton polarization vanish, corresponding to the vacuum limit $T \to 0$, resulting in no polarization.

$$\lambda_{ heta} \sim rac{M}{T}$$

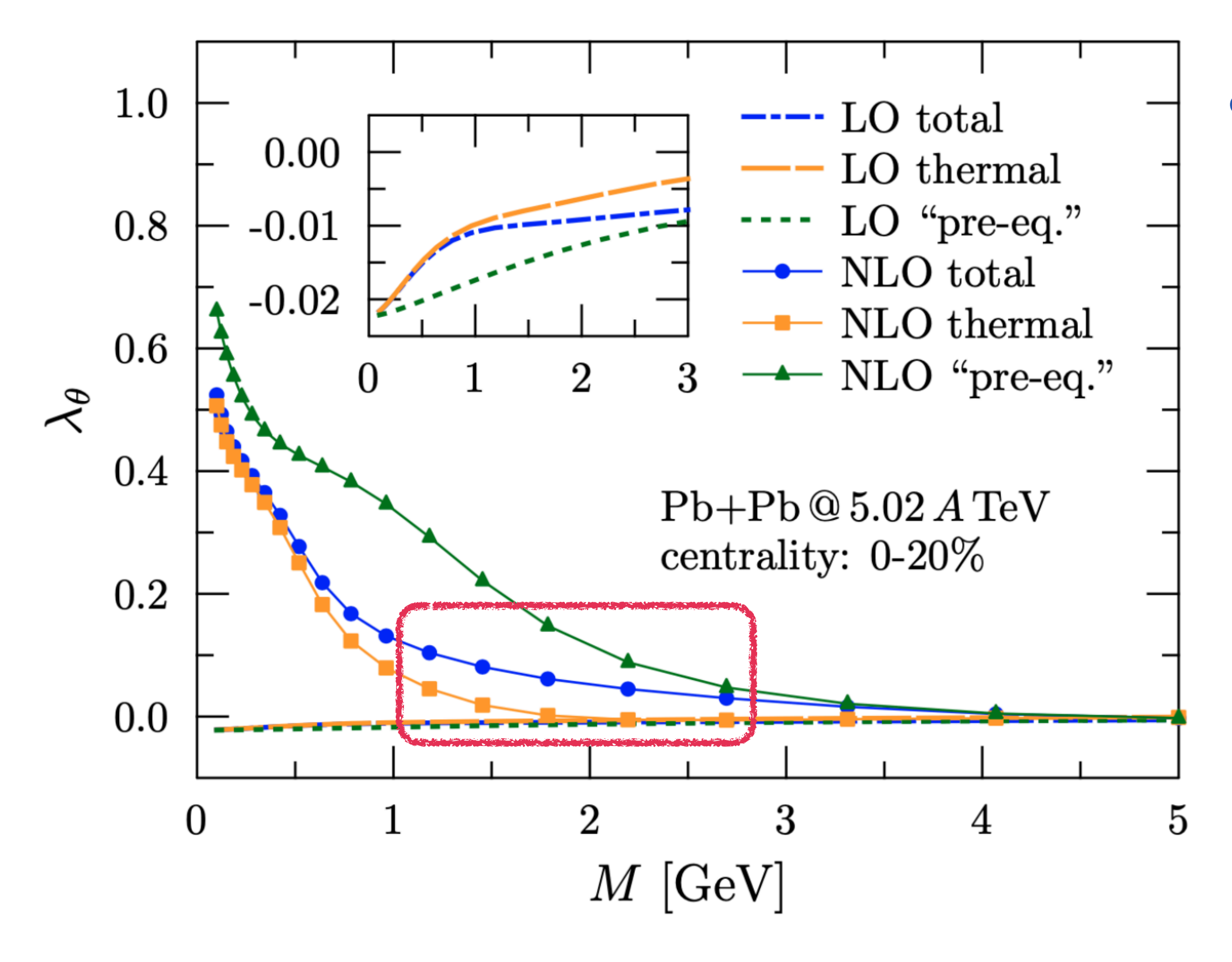


- NLO and LO results differ significantly.
 - $M \rightarrow 0$, the virtual photon behaves like a real photon, exhibiting only transverse polarization.
 - $M \to \infty$, both LO and NLO dilepton polarization vanish, corresponding to the vacuum limit $T \to 0$, resulting in no polarization.
- λ_{θ} also depends on the flow effects.

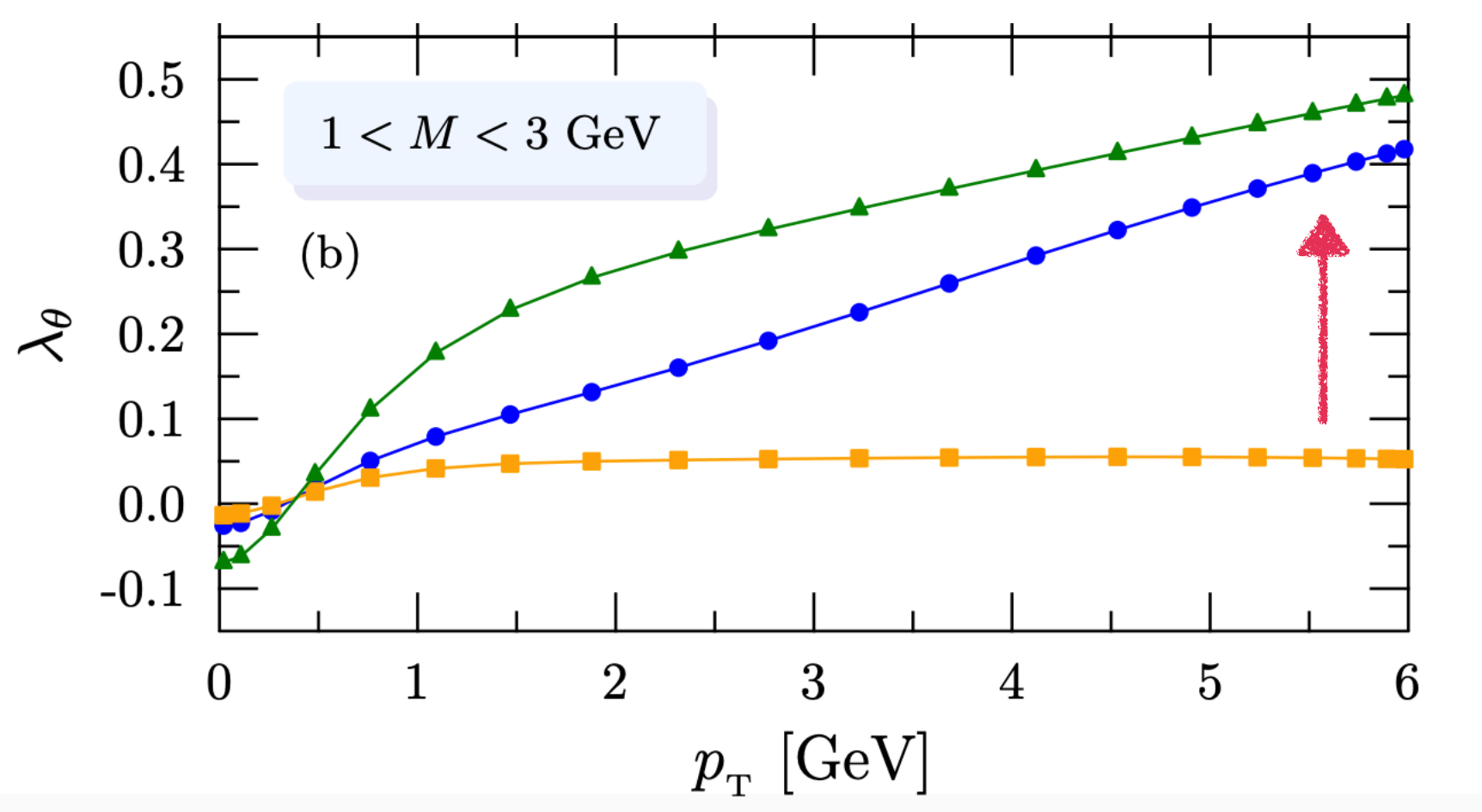




- NLO and LO results differ significantly.
 - $M \rightarrow 0$, the virtual photon behaves like a real photon, exhibiting only transverse polarization.
 - $M \to \infty$, both LO and NLO dilepton polarization vanish, corresponding to the vacuum limit $T \to 0$, resulting in no polarization.
- λ_{θ} also depends on the flow effects.
- λ_{θ} is sensitive to early-time dynamics.



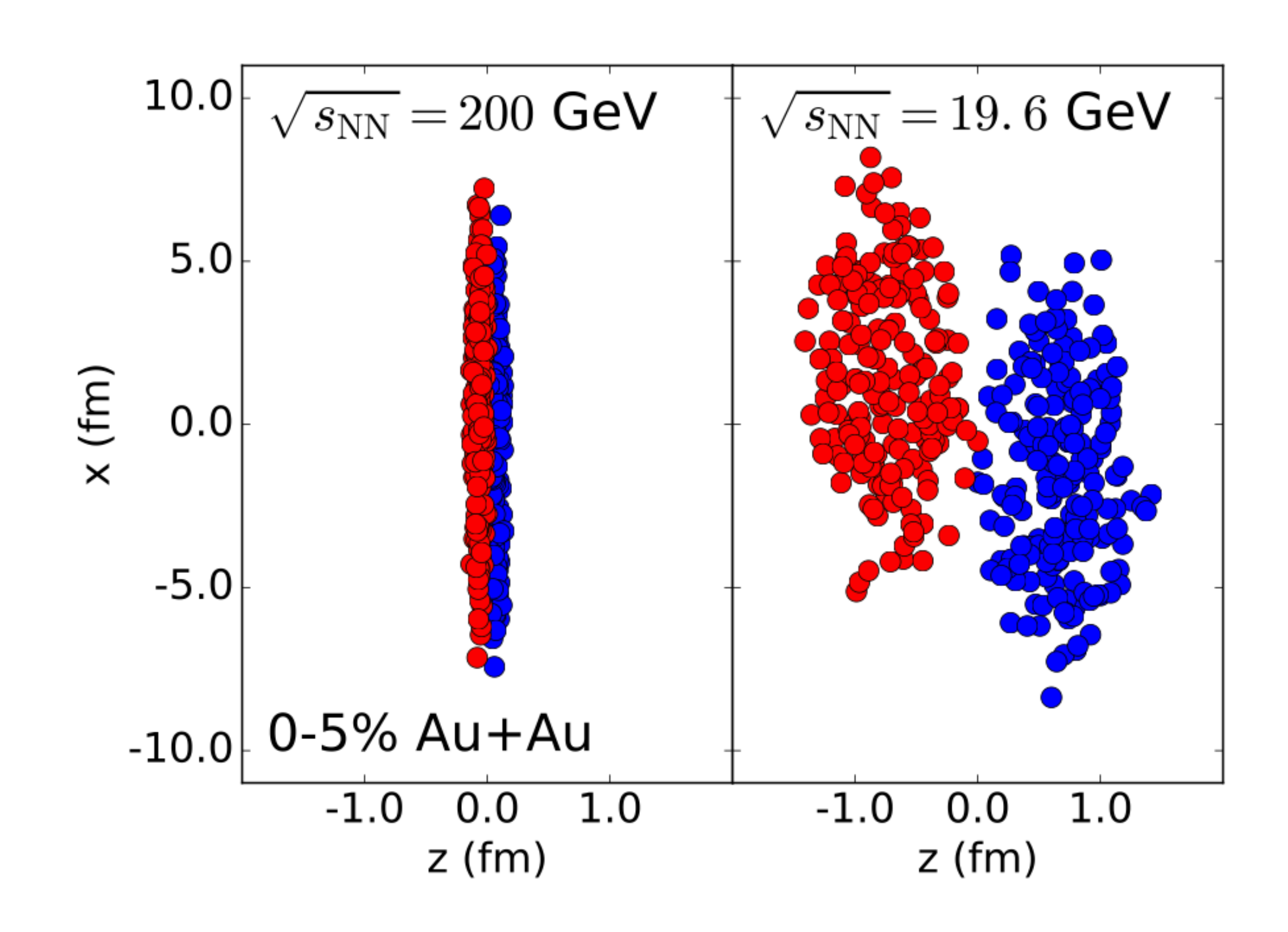
- NLO and LO results differ significantly in the limit $M \to 0$.
 - $M \rightarrow 0$, the virtual photon behaves like a real photon, exhibiting only transverse polarization.
 - $M \to \infty$, both LO and NLO dilepton polarization vanish, corresponding to the vacuum limit $T \to 0$, resulting in no polarization.
- λ_{θ} also depends on the flow effects.
- λ_{θ} is sensitive to early-time dynamics.



Outline

- Introduction
- Dileptons in the Pre-equilibrium Stage
- Dilepton polarization
- Dilepton and photons at RHIC-BES
- Summary

Heavy ion collision at RHIC-BES energy



80 (E802,E877, E917)

SPS (NA49)

60 62.4 GeV

200 GeV (BRAHMS)

62.4 y_B

62.4 y_B

Longer overlap time

Finite baryon density

3D-Glauber+MUSIC+URQMD

Усм

 τ [fm] ≈ 0.5

3D dynamical MC-Glauber model

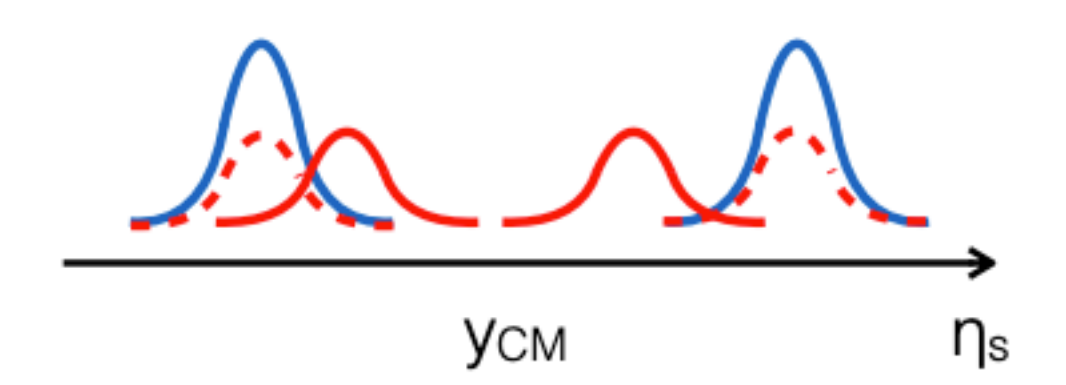
~ 400

T[MeV]

• Transverse geometry is determined by MC-Glauber Model.

• Longitudinal dynamics is modelled by a string tension.

Baryon density is deposited at the string ends or string junctions



energy density inside the string

~ 270

~ 155

3D-Glauber+MUSIC+URQMD

τ [fm]

 ≈ 0.5

 ≈ 10

T[MeV]

3D dynamical MC-Glauber model

~ 400

- Transverse geometry is determined by MC-Glauber Model.
- Longitudinal dynamics is modelled by a string tension.

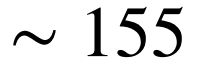
Hydrodynamic evolution: MUSIC

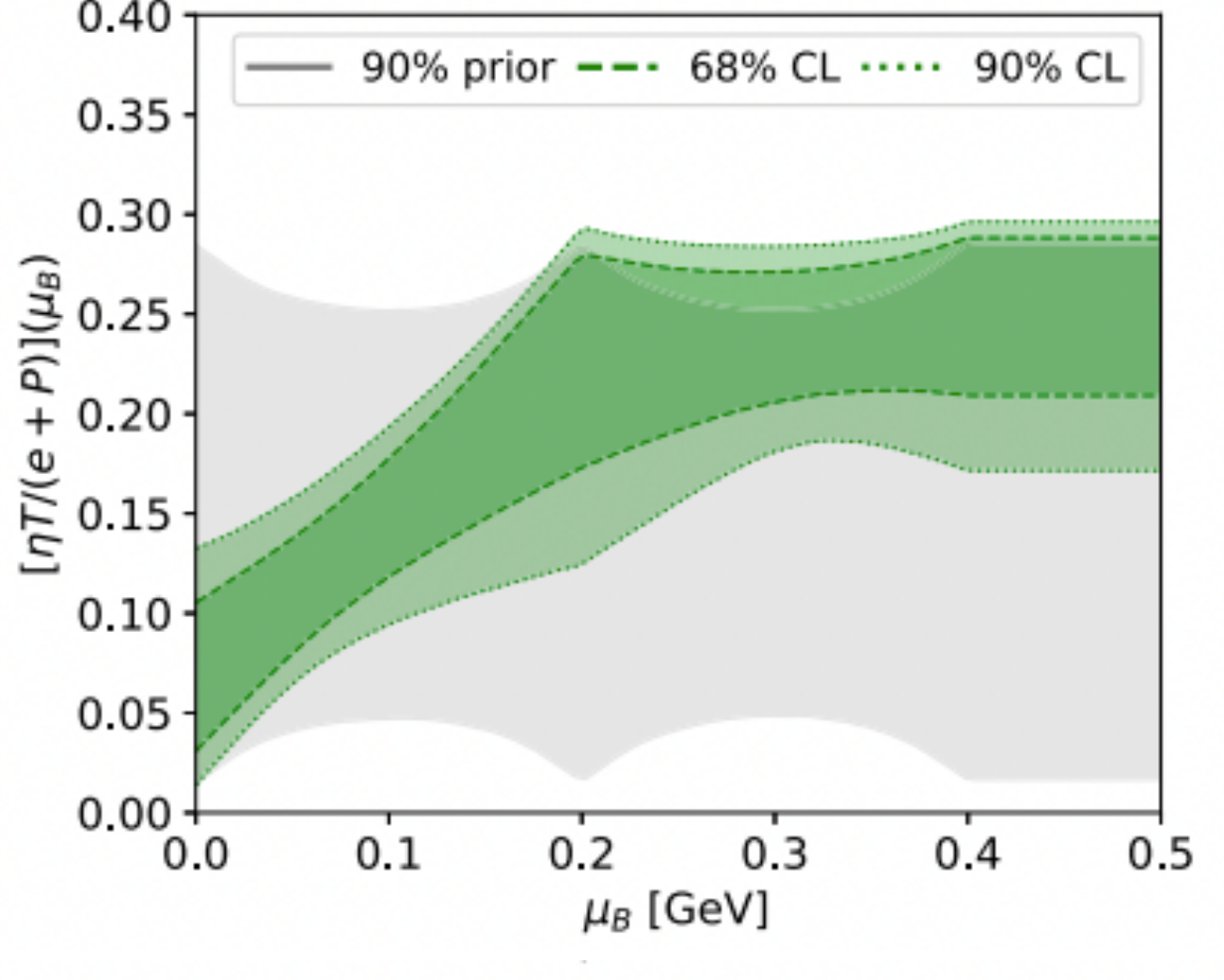
$$\partial_{\mu}T^{\mu\nu} = J^{\nu}_{\text{source}}$$

$$\partial_{\mu}J^{\mu} = \rho_{\text{source}}$$

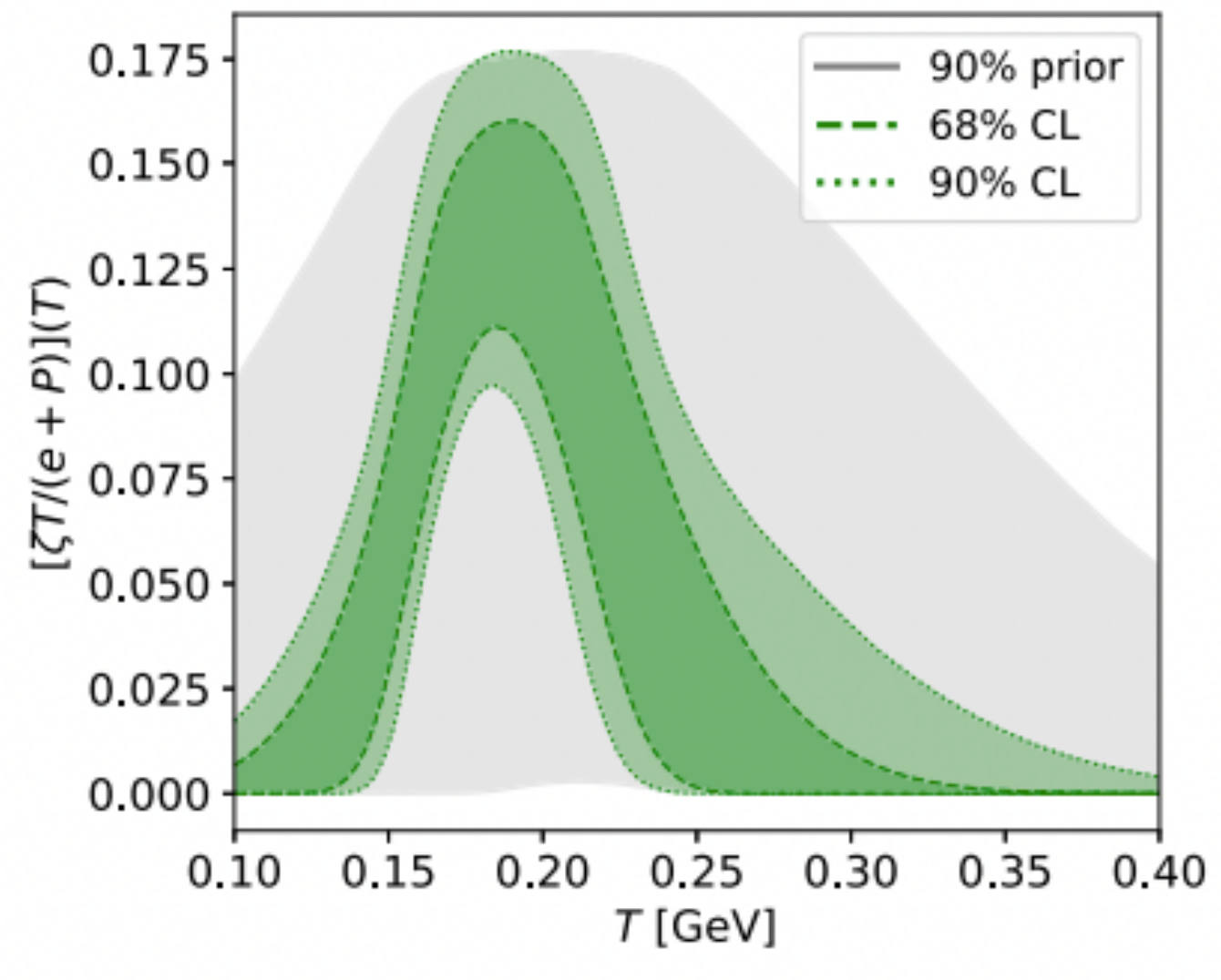
- $\eta(\mu_B), \zeta(T, \mu_B)$
- NEOS $(T, n_b, n_s = 0, n_Q = 0.4n_b)$

Hadronic cascade: URQMD





A piece-wise parameterization $\eta/s(\mu_B)$



A two-piece asymmetric Gaussian parameterization $\zeta/s(T)$

[Schenke, Jeon and Gale, PRC 82, 014903 (2010), Schenke, Jeon and Gale, PRL 106, 042301 (2011), Denicol, Gale, Jeon, Monnai, Schenke and Shen, PRC 98, 034916 (2018), Jahan, Roch and Shen, PRC 110.054905 (2024)]

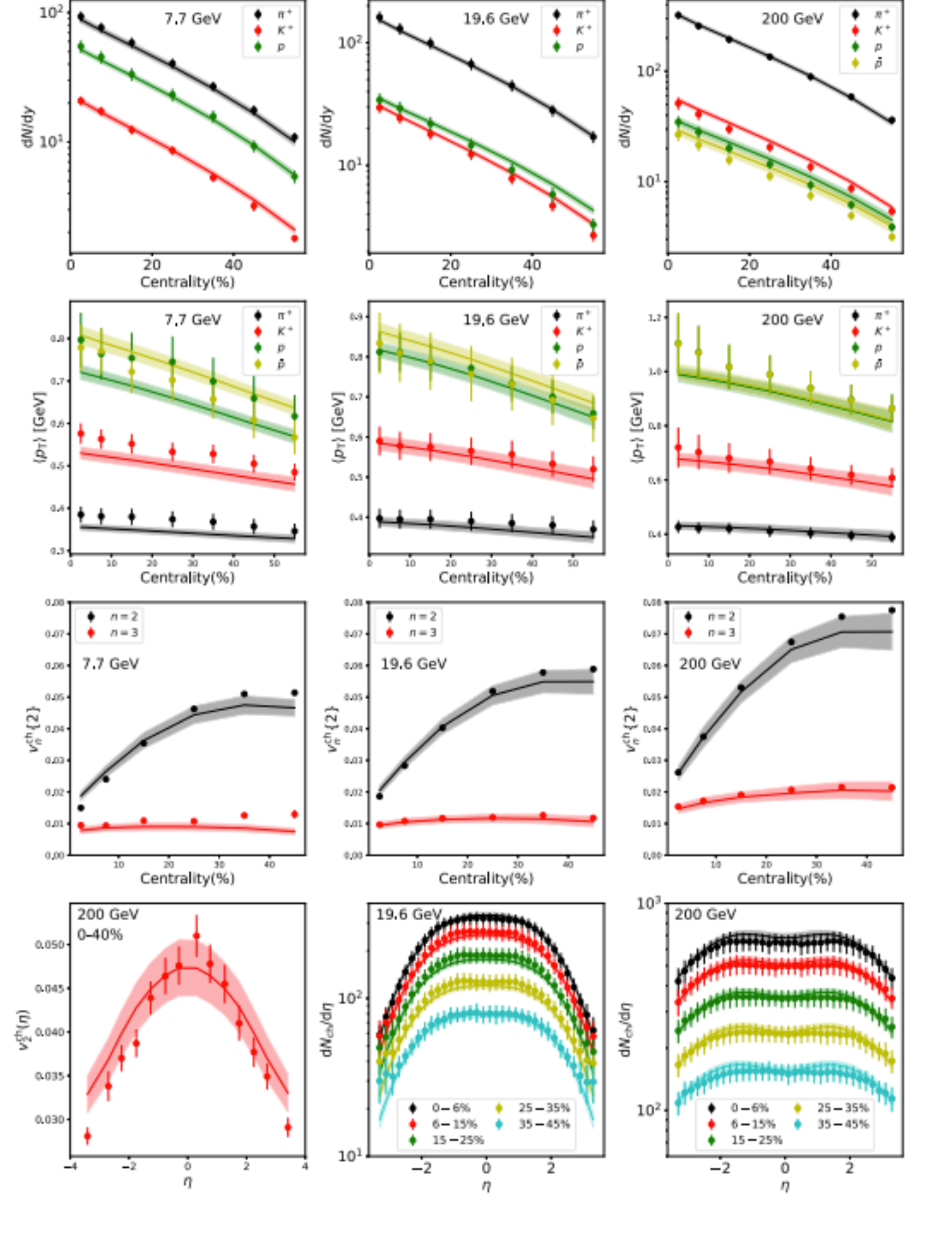
Bayesian inference at RHIC-BES energies

TABLE I. The 20 model parameters and their prior ranges.

Parameter	Prior	Parameter	Prior
$B_G [\mathrm{GeV}^{-2}]$	[1, 25]	$lpha_{ m string\ tilt}$	[0, 1]
$lpha_{ m shadowing}$	[0, 1]	$lpha_{ m preFlow}$	[0, 2]
$y_{ m loss,2}$	[0, 2]	η_0	[0.001, 0.3]
$y_{ m loss,4}$	[1, 3]	η_2	[0.001, 0.3]
$y_{ m loss,6}$	[1,4]	η_4	[0.001, 0.3]
$\sigma_{y_{ m loss}}$	[0.1, 0.8]	$\zeta_{ m max}$	[0, 0.2]
$lpha_{ m rem}$	[0, 1]	$T_{\zeta,0} \ [{ m GeV}]$	[0.15, 0.25]
λ_B	[0, 1]	$\sigma_{\zeta,+} \ [{ m GeV}]$	[0.01, 0.15]
$\sigma_x^{ m string} \; [{ m fm}]$	[0.1, 0.8]	$\sigma_{\zeta,-} \ [{ m GeV}]$	[0.005, 0.1]
$\sigma_{\eta}^{ m string}$	[0.1, 1]	$e_{ m sw}~[{ m GeV/fm^3}]$	[0.15, 0.5]

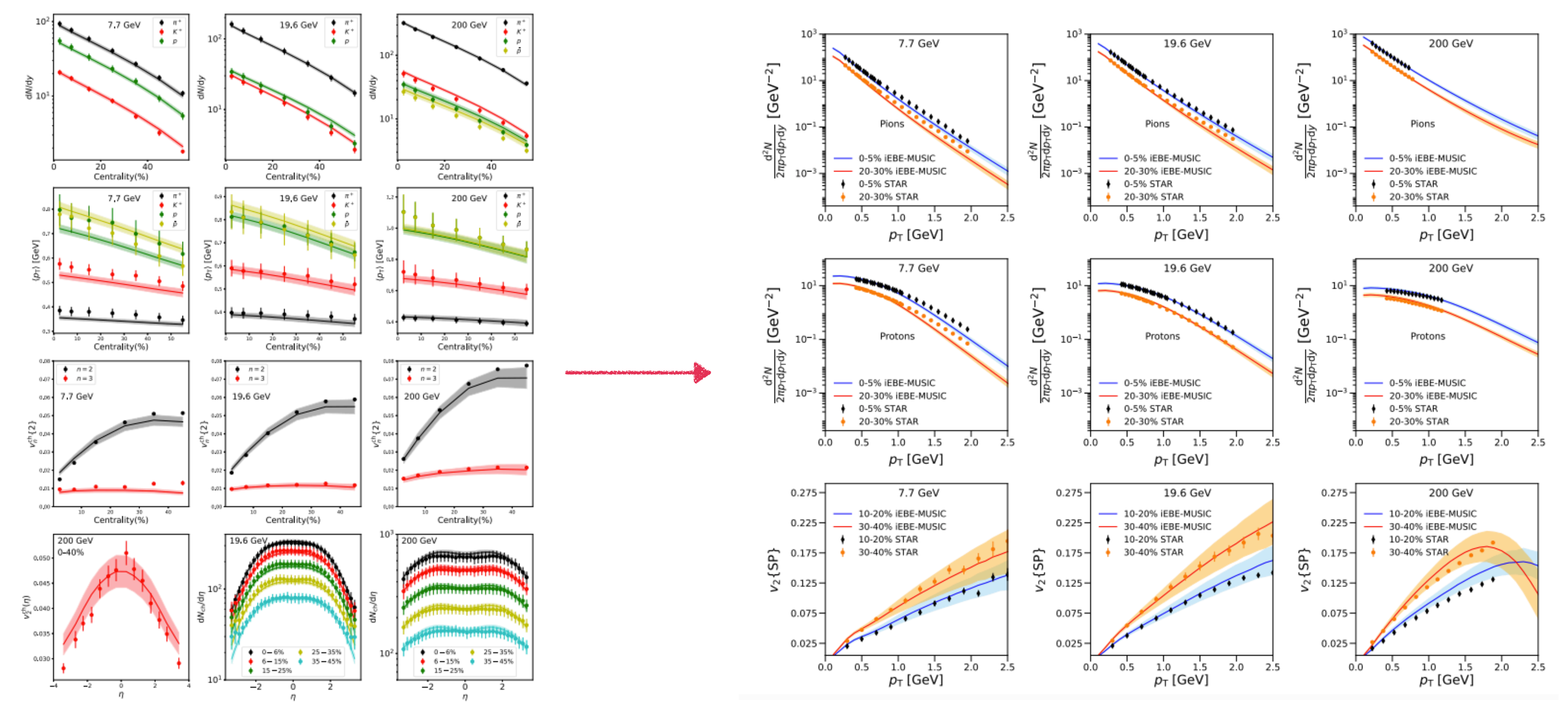
20 model parameters +544 data points

$\sqrt{s_{\rm NN}}$ [GeV]	STAR	PHOBOS	
200	$dN/dy(\pi^+, K^+, \bar{p}, p)$ [72]	$dN_{ch}/d\eta$ [73]	
200	$\langle p_{\mathrm{T}} \rangle (\pi^+, K^+, p, \bar{p}$ [72]	$v_2^{\rm ch}(\eta)$ [74]	
200	$v_2^{\text{ch}}\{2\}$ [75], $v_3^{\text{ch}}\{2\}$ [76]		
19.6	$dN/dy(\pi^+, K^+, p)$ [77]	$\mathrm{d}N_{\mathrm{ch}}/\mathrm{d}\eta$ [73]	
19.6	$\langle p_{\rm T} \rangle (\pi^+, K^+, p, \bar{p}) [77]$		
19.6	$v_2^{\text{ch}}\{2\}$ [75], $v_3^{\text{ch}}\{2\}$ [76]		
7.7	$dN/dy(\pi^+, K^+, p)$ [77]		
7.7	$\langle p_{\rm T} \rangle (\pi^+, K^+, p, \bar{p}) [77]$		
7.7	$v_2^{\text{ch}}\{2\}$ [75], $v_3^{\text{ch}}\{2\}$ [76]		



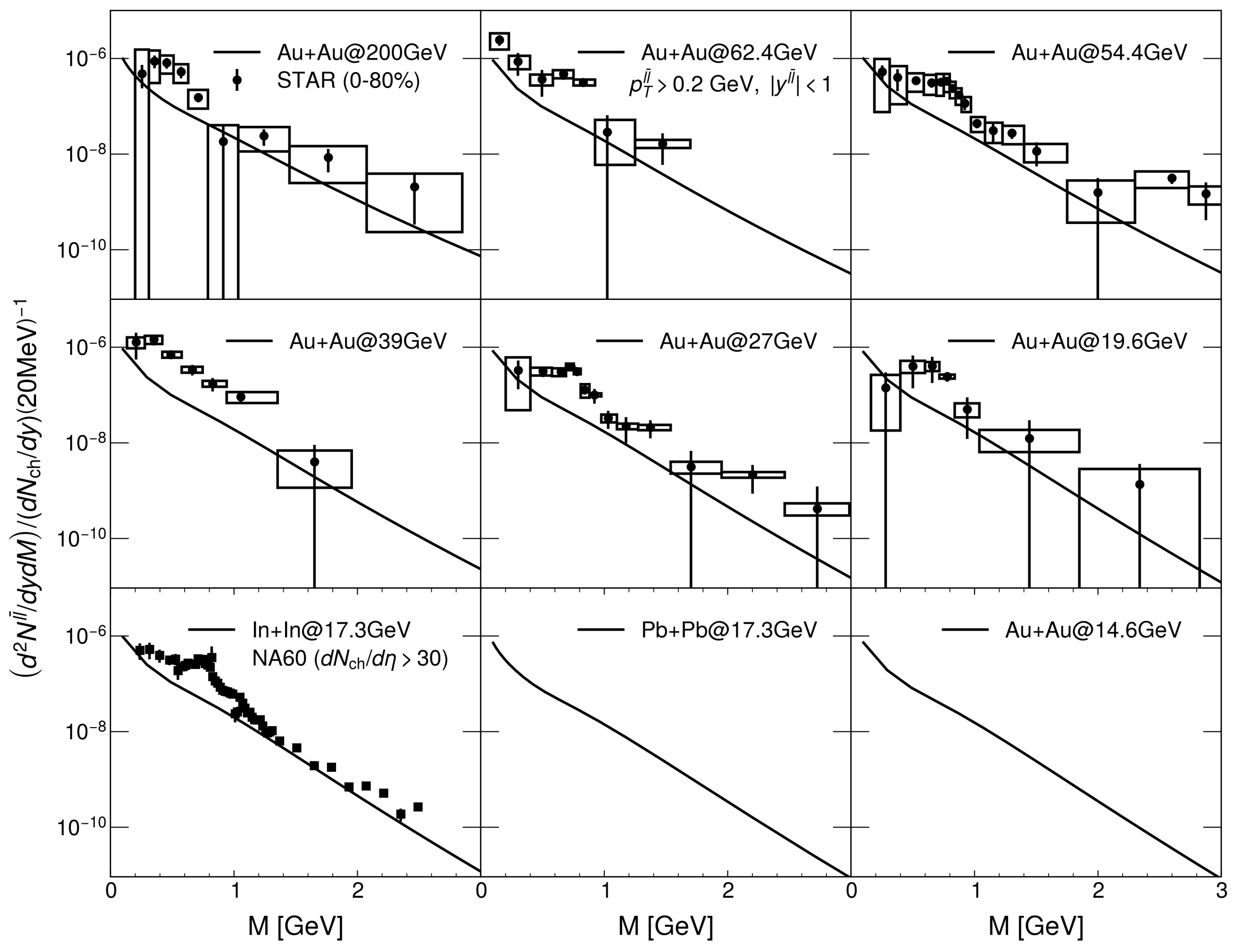
[PRC 110. 054905 (2024)]

Bayesian inference at RHIC-BES energies



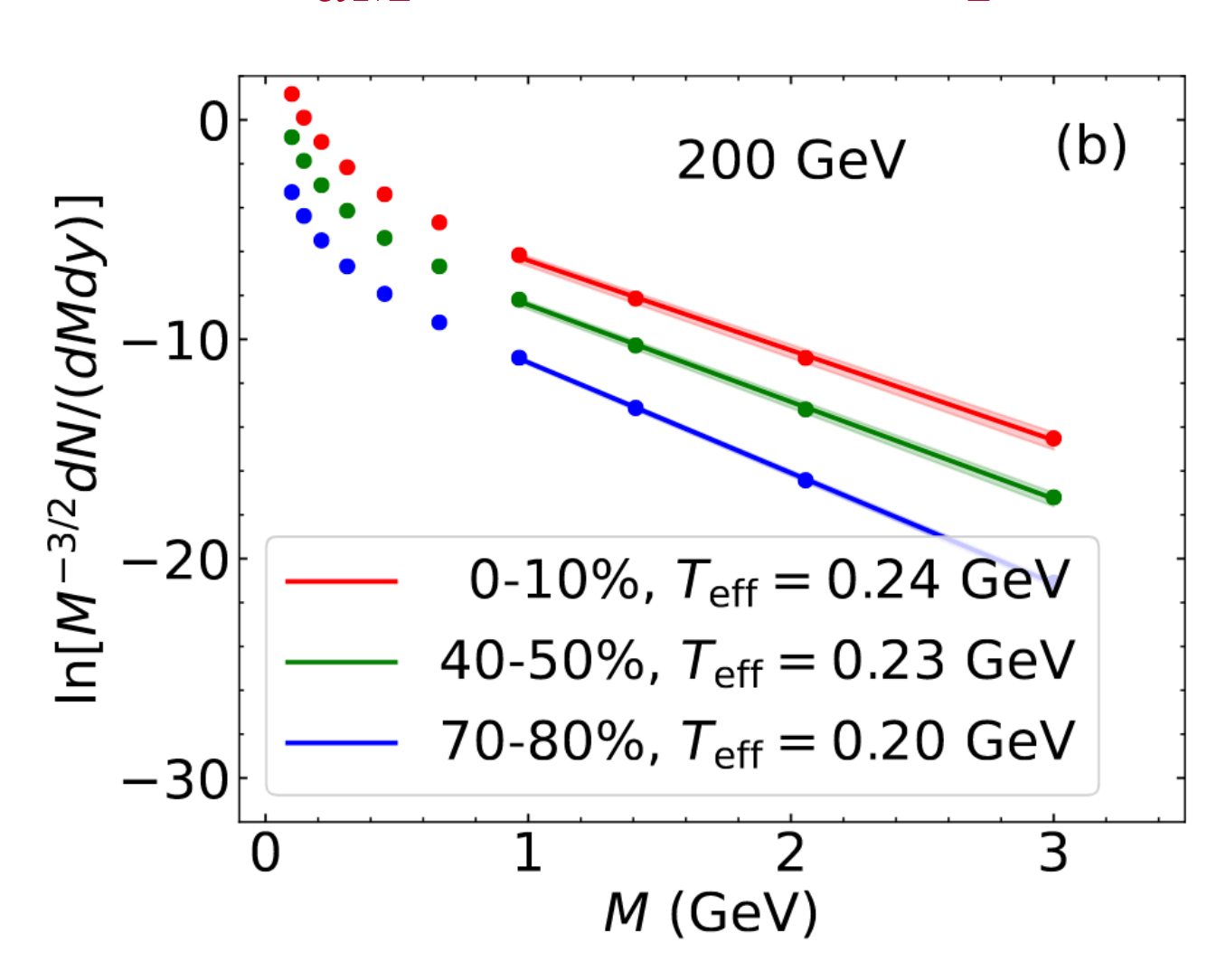
• After model calibration, the full model simulation based on the posterior distribution provides a prediction for p_T -differential observables.

Thermal dilepton as a QGP thermometer



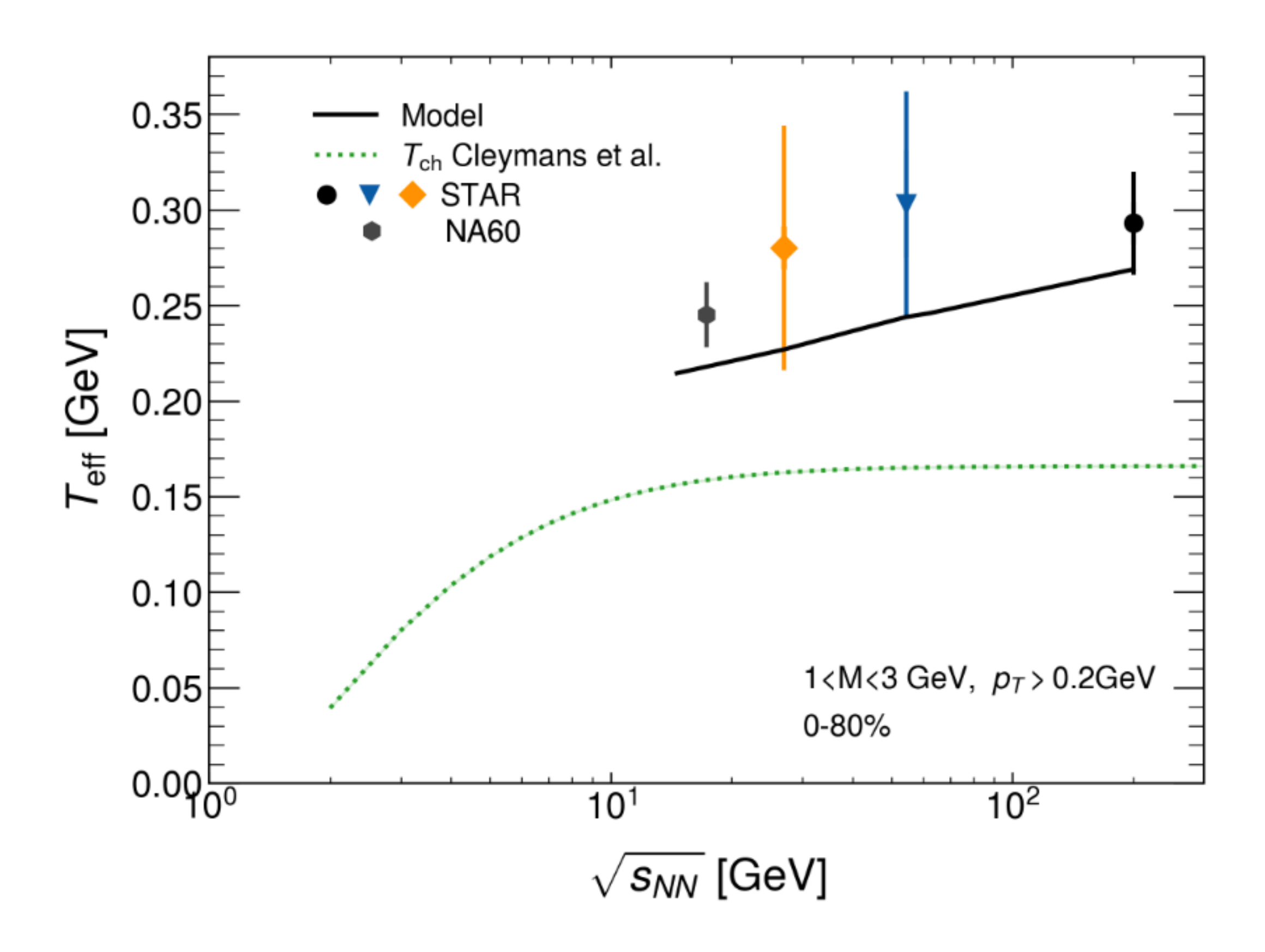
- The model calculations show reasonable agreement with the STAR preliminary data at RHIC-BES energies.
- As a plasma thermometer, the temperature T can be extracted by fitting the spectrum in the range 1 < M < 3 GeV.

$$\frac{dN_{\ell\bar{\ell}}}{dM} \propto (MT)^{\frac{3}{2}} \exp\left(-\frac{M}{T}\right).$$



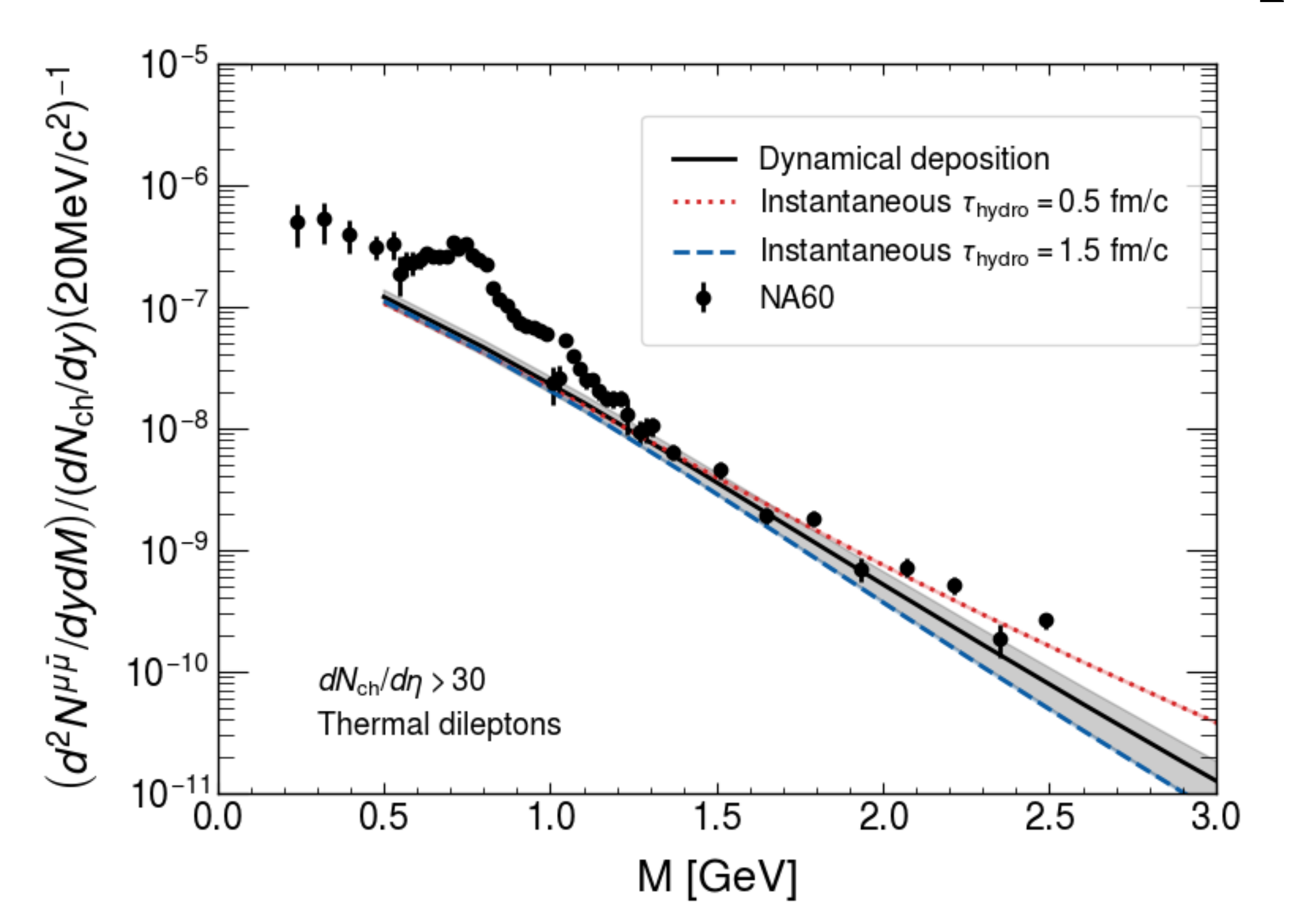
 \bullet T_{eff} : an average value over the temperatures of the fluid cells.

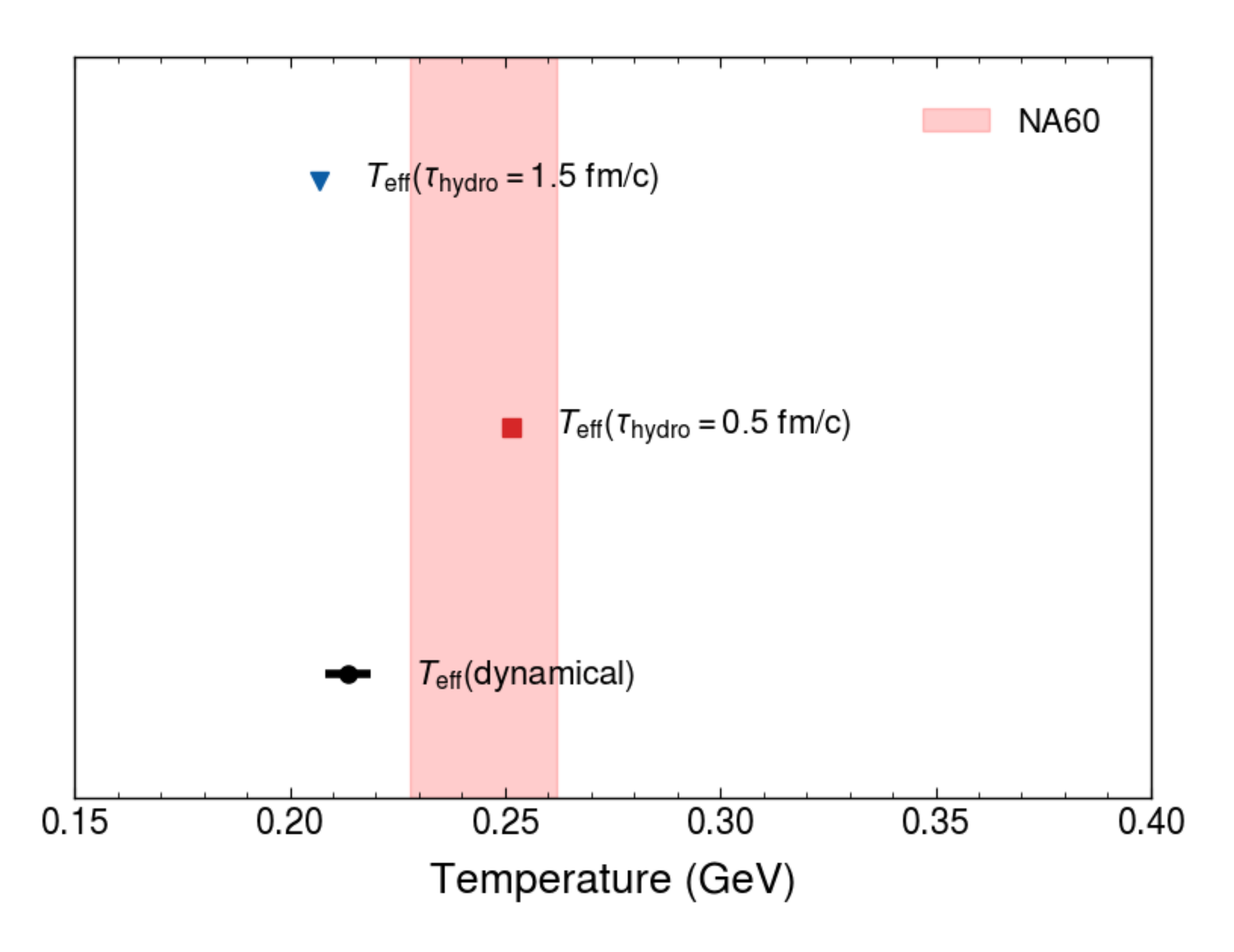
Thermal dilepton as a QGP thermometer



- Temperature estimates from model simulations are statistically consistent with experimental data measurements.
- Additional components: pre-equilibrium evolution, non-equilibrium corrections to rates...

How well we can extract the temperature?





- Initialization affects the slope of dilepton yield and the extracted temperature.
- The dynamical initialization lies between the two instantaneous limits, and is closer to the profile at $\tau_{\text{hydro}} = 1.5 \text{ fm/c}$.

Photon Sources

τ [fm]

 ≈ 0.5

 ≈ 10

T[MeV]

3D dynamical MC-Glauber model

~ 400

~ 270

- Transverse geometry is determined by MC-Glauber Model.
- Longitudinal dynamics is modeled by a string tension.

Hydrodynamic evolution: MUSIC

$$\partial_{\mu}T^{\mu\nu} = J^{\nu}_{\text{source}}$$

$$\partial_{\mu}J^{\mu} = \rho_{\text{source}}$$

- $\eta(\mu_B), \zeta(T, \mu_B)$
- NEOS $(T, n_b, n_s = 0, n_Q = 0.4n_b)$

Hadronic cascade: URQMD

~ 155

Prompt photon

$$E\frac{d^3N_{AA}}{d^3p} = \frac{N_{coll}}{\sigma_{in}^{pp}} \sum_{a,b,c,d} f_a^p(x_a, Q_{\text{fact}}) \otimes f_b^p(x_b, Q_{\text{fact}}) \otimes \hat{\sigma}(Q_{\text{ren}}) \otimes D_{h/c}(z_c, Q_{\text{frag}}).$$

Thermal photon

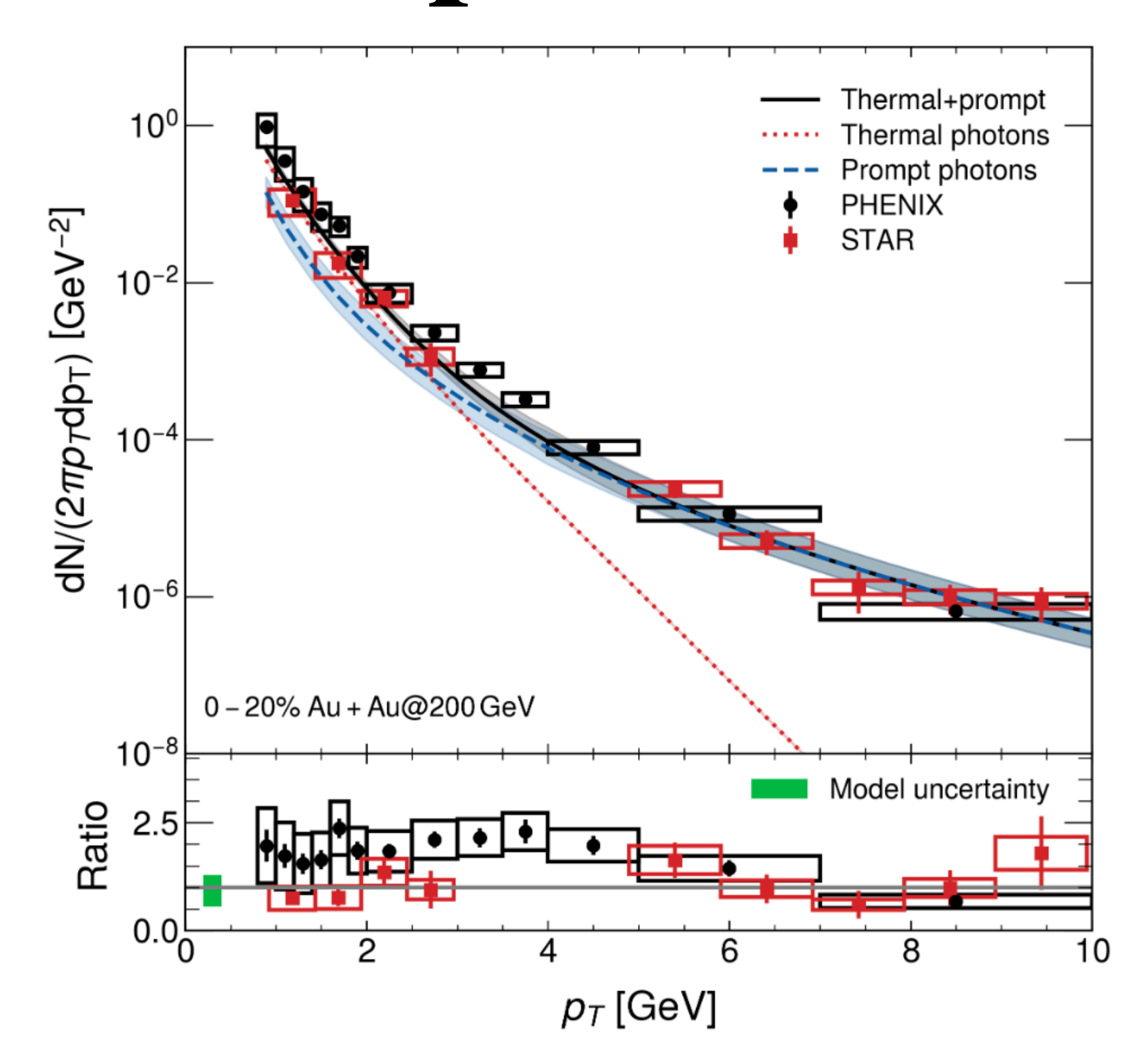
$$E\frac{dN_{\gamma}}{d^{3}p} = \int d^{4}x \frac{d\Gamma_{\gamma}}{d^{3}p} \left(p, T(x), u^{\mu}(x), \mu_{B}(x), \ldots\right).$$

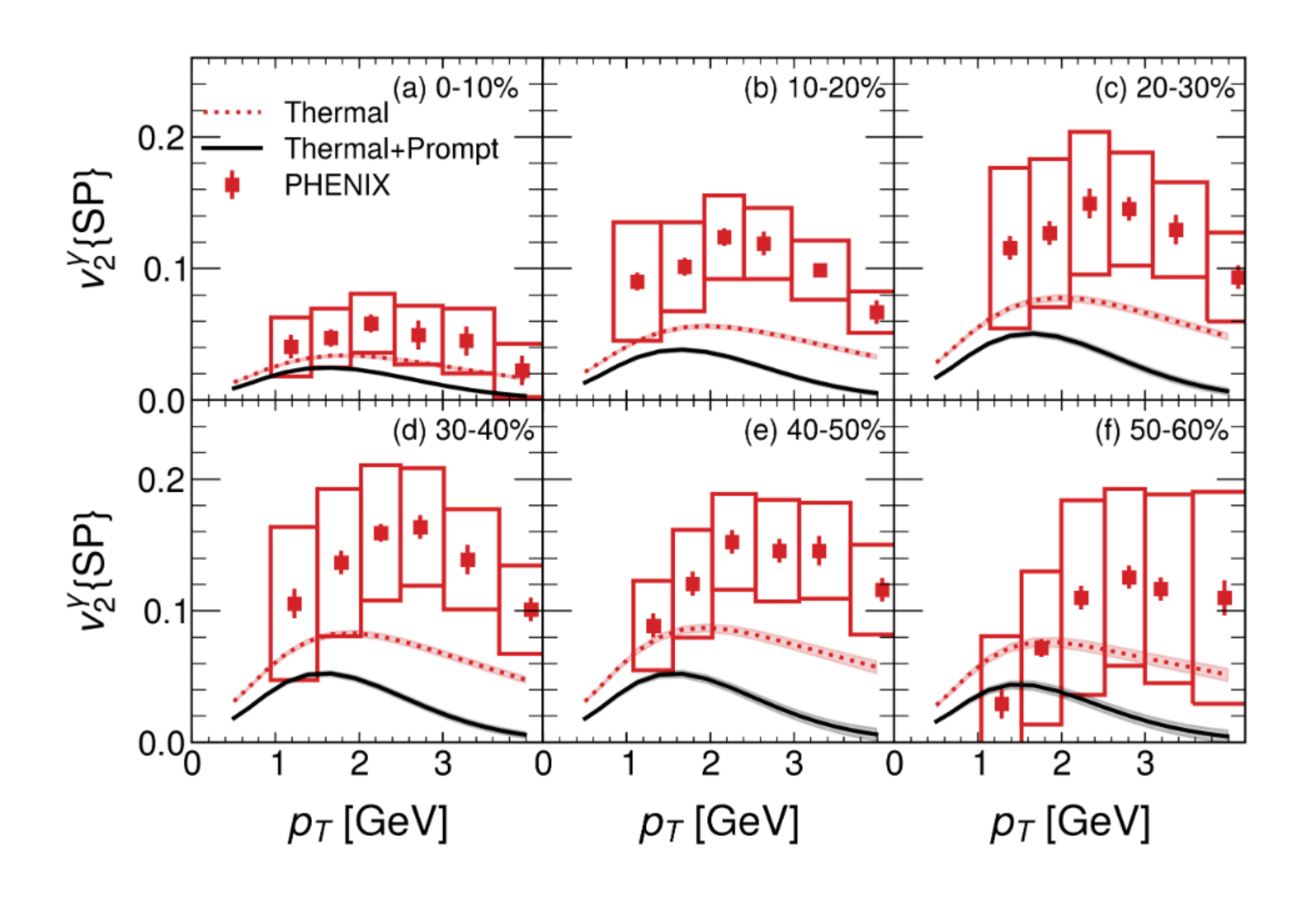
Photon:

- QGP rates: Compton scatterings, $q\bar{q}$ annihilation & LPM effects
- Hadronic rates: meson scatterings & baryon interactions

[Paquet, Shen, Denicol, Luzum, Schenke, Jeon and Gale PRC 93, 044906 (2016)]

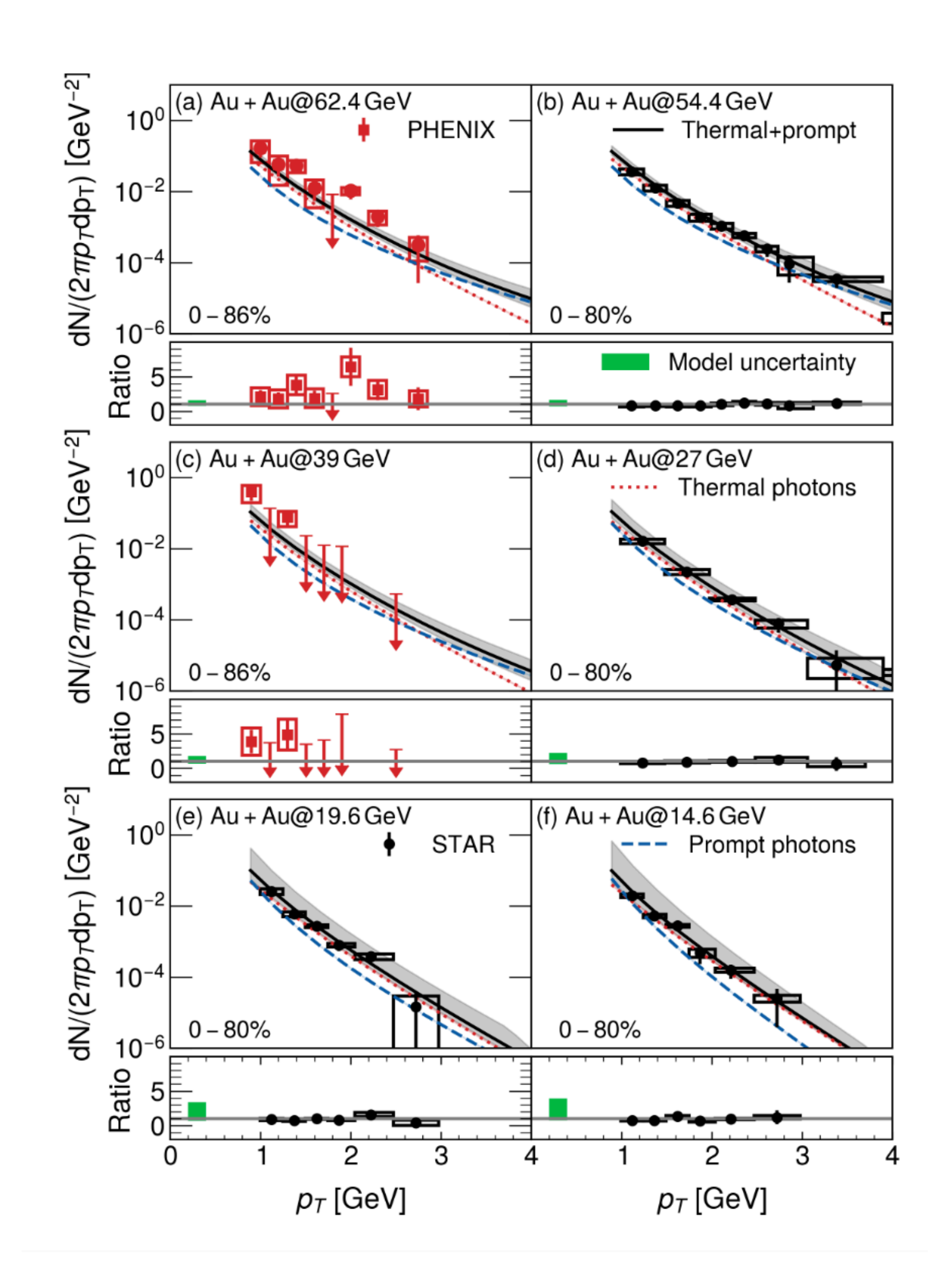
Photon production and flow





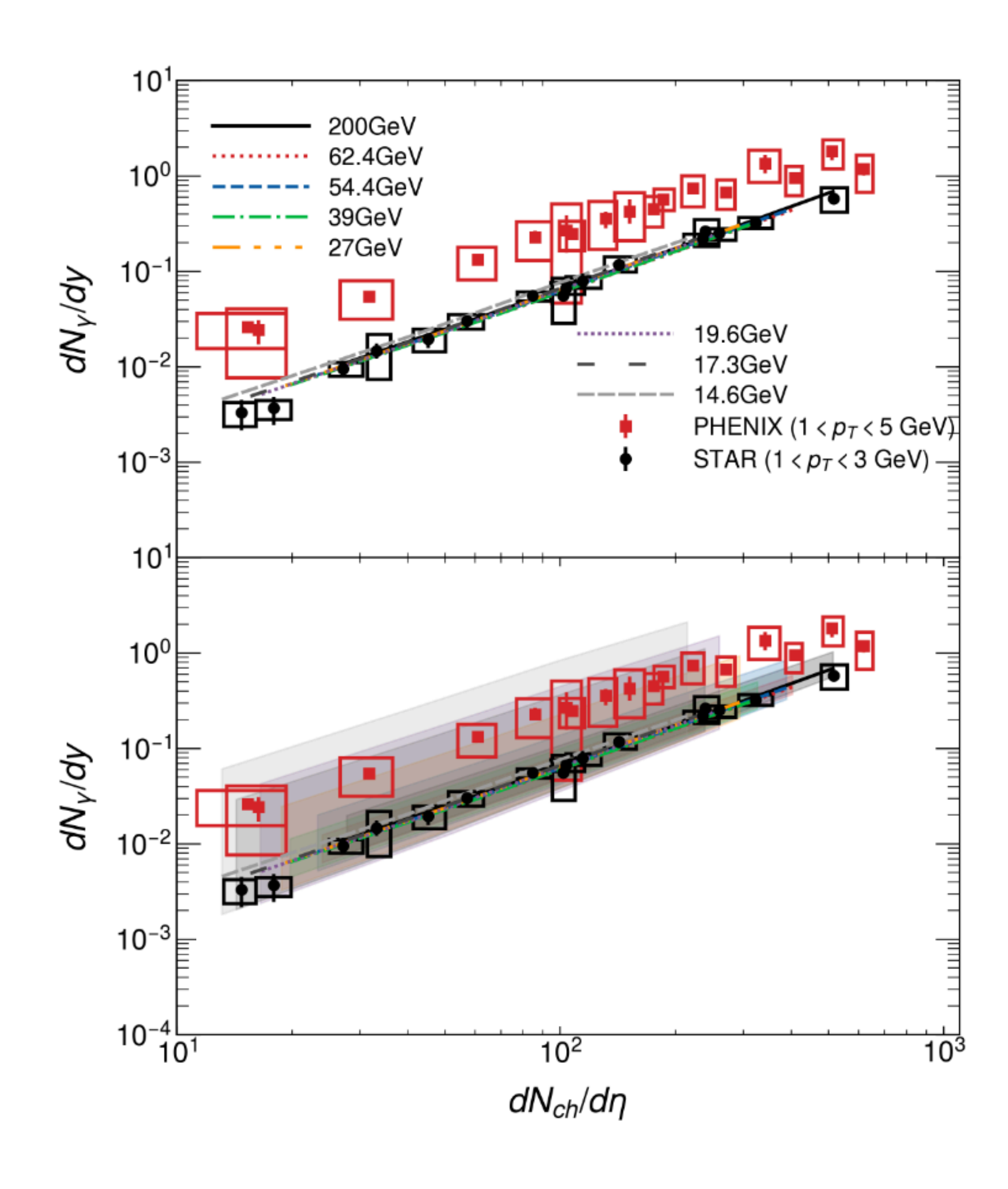
- At high p_T ($p_T > 4$ GeV), prompt photon production follows N_{coll} scaling, showing good agreement with STAR& PHENIX data.
- Thermal photon dominates the low- p_T region ($p_T < 3$ GeV).
- Thermal photons have sizeable elliptic flow, but the direct photon flow is suppressed by prompt photon contribution.
- Direct photon puzzle still unsolved

Photon production at the RHIC-BES



- The slope of the direct photon spectrum steepens as the collision energy decreases, due to reduced blue-shift effects and lower temperatures.
- Thermal photons contribute significantly at low energies, but the uncertainty of the prompt photon contribution is still large.
- The measurements of prompt photons in low-energy p+p collisions are essential to constrain and extract the thermal component.

Scaling of direct photon yield



- Universal scaling behaviour has been observed in the direct photon yield.
- With a fixed scale factor ($\lambda = 0.5$) for prompt photons, the scaling better matches the STAR data.
- After accounting for the uncertainty in prompt photon production, the theoretical results are not sufficiently precise to distinguish between the STAR and PHENIX data.

Summary

- Dilepton observables offer a valuable opportunity to probe the quark production during the pre-equilibrium stage.
- Including NLO corrections is essential for obtaining a physically meaningful dilepton polarization prediction.
- Dileptons act as effective thermometers of the QGP medium.
- Current theoretical models predict prompt photons with large uncertainties, demanding more inputs from experimental measurements.
- A new era of multi-messenger heavy-ion physics is emerging.

Thank you for your attention!